Cell Reports

Article

Correction of amygdalar dysfunction in a rat model of fragile X syndrome

Graphical abstract

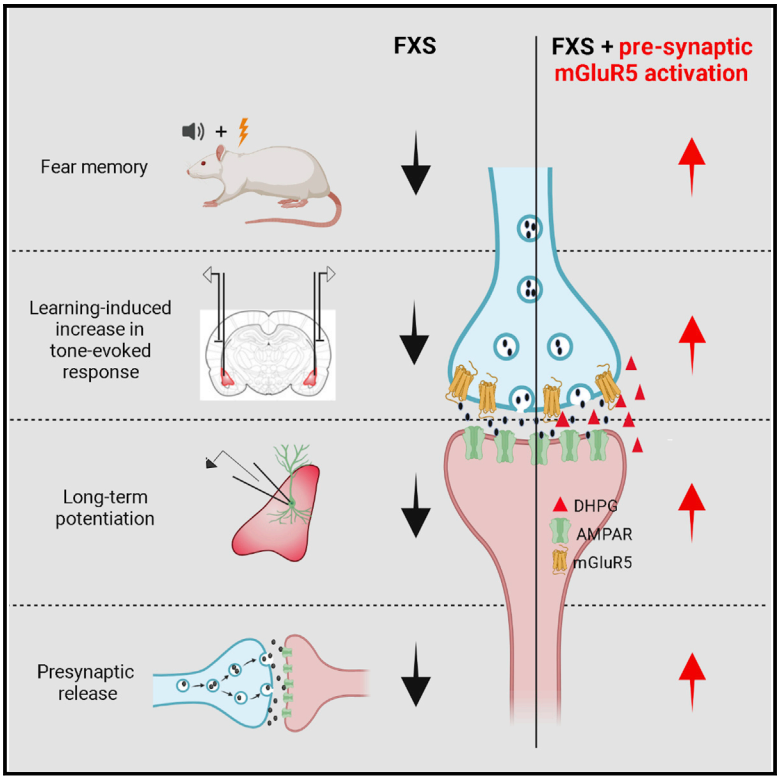

Highlights

- Recall of conditioned fear is deficient in a rat model of fragile X syndrome
- Synaptic transmission, and plasticity underlying fear learning, is reduced in the BLA
- mGluR5 receptors are present in presynaptic terminals of the BLA
- Activation of BLA mGluR5 restores synaptic plasticity and fear learning in FXS rats

Authors

Giselle Fernandes, Pradeep K. Mishra, Mohammad Sarfaraz Nawaz, ..., Erin M. Schuman, Peter C. Kind, Sumantra Chattarji

Correspondence

shona@ncbs.res.in

In brief

Fernandes et al. investigate the synaptic basis of deficient conditioned fear and its reversal in FXS rats. They find presynaptic mGluR5 in the amygdala, activation of which restores normal synaptic transmission, plasticity, and fear learning. This highlights the importance of circuit-specific differences in FXS pathophysiology and mGluR-based therapeutic strategies.

Fernandes et al., 2021, Cell Reports *37*, 109805
October 12, 2021
https://doi.org/10.1016/j.celrep.2021.109805

CellPress

Cell Reports

CellPress
OPEN ACCESS

Article

Correction of amygdalar dysfunction in a rat model of fragile X syndrome

Giselle Fernandes,[1,8,9] Pradeep K. Mishra,[1,2,9] Mohammad Sarfaraz Nawaz,[1,2] Paul G. Donlin-Asp,[4] Mohammed Mostafizur Rahman,[5] Anupam Hazra,[1,2] Sonal Kedia,[6] Aiman Kayenaat,[1,2,7] Dheeraj Songara,[1] David J.A. Wyllie,[2,3] Erin M. Schuman,[4] Peter C. Kind,[2,3] and Sumantra Chattarji[1,2,3,10,*]

[1]National Centre for Biological Sciences, TIFR, Bangalore 560065, India
[2]Centre for Brain Development and Repair, Institute for Stem Cell Biology and Regenerative Medicine, Bangalore 560065, India
[3]Simons Initiative for the Developing Brain and Centre for Discovery Brain Sciences, University of Edinburgh, Edinburgh EH8 9XD, UK
[4]Max Planck Institute for Brain Research, Frankfurt, Germany
[5]Department of Molecular and Cellular Biology, Center for Brain Science, Harvard University, Cambridge, MA, USA
[6]Department of Biology, Brandeis University, Waltham, MA, USA
[7]University of Transdisciplinary Health Sciences and Technology, Bangalore 560064, India
[8]Present address: Departments of Neurobiology, Psychology, Psychiatry, and Biobehavioral Sciences, Integrative Center for Learning and Memory, Brain Research Institute, UCLA, Los Angeles, CA 90095, USA
[9]These authors contributed equally
[10]Lead contact
*Correspondence: shona@ncbs.res.in
https://doi.org/10.1016/j.celrep.2021.109805

SUMMARY

Fragile X syndrome (FXS), a commonly inherited form of autism and intellectual disability, is associated with emotional symptoms that implicate dysfunction of the amygdala. However, current understanding of the pathogenesis of the disease is based primarily on studies in the hippocampus and neocortex, where FXS defects have been corrected by inhibiting group I metabotropic glutamate receptors (mGluRs). Here, we observe that activation, rather than inhibition, of mGluRs in the basolateral amygdala reverses impairments in a rat model of FXS. FXS rats exhibit deficient recall of auditory conditioned fear, which is accompanied by a range of *in vitro* and *in vivo* deficits in synaptic transmission and plasticity. We find presynaptic mGluR5 in the amygdala, activation of which reverses deficient synaptic transmission and plasticity, thereby restoring normal fear learning in FXS rats. This highlights the importance of modifying the prevailing mGluR-based framework for therapeutic strategies to include circuit-specific differences in FXS pathophysiology.

INTRODUCTION

Fragile X syndrome (FXS), a leading genetic cause of intellectual disability and autism spectrum disorder, is caused by the absence of the fragile X mental retardation protein (FMRP) produced by the fragile X mental retardation1 (*FMR1*) gene. One key feature of the symptoms of FXS is abnormal emotional behavior, and clinical evidence points to the amygdala's contribution to these affective symptoms. Neuroimaging revealed that men with the *FMR1* premutation exhibit reduced activation in the amygdala in response to fearful faces (Hessl et al., 2007). These men also had impaired startle potentiation while viewing fearful faces, implicating amygdalar dysfunction. However, earlier mechanistic analyses using rodent models of FXS focused almost exclusively on the hippocampus and neocortex, not the amygdala. These studies gave rise to the "mGluR theory" of FXS, an influential framework for understanding the synaptic and molecular underpinnings of FXS (Bear et al., 2004). This theory proposes that various symptoms of the disorder are the consequences of unchecked activation of mGluR5, a group 1 metabotropic glutamate receptor. A major observation leading to this theory is that mGluR5 is involved in long-term depression (LTD) (Fitzjohn et al., 2001; Palmer et al., 1997), a form of hippocampal synaptic plasticity that is elevated in the *Fmr1* knockout (*Fmr1*$^{-/y}$) mouse (Hou et al., 2006; Huber et al., 2002; Nakamoto et al., 2007; Till et al., 2015). This is significant in light of the contrasting nature of mGluR-dependent synaptic plasticity in the hippocampus versus amygdala. In the lateral amygdala, mGluR5 mediates long-term potentiation (LTP) of synaptic strength (Rodrigues et al., 2002). Although hippocampal mGluR-LTD is enhanced in *Fmr1*$^{-/y}$ mice, the opposite effect—impaired LTP—was reported in the amygdala of these mice (Suvrathan et al., 2010). In other words, the direction of synaptic plasticity mediated by mGluRs (i.e., LTP versus LTD) and its dysfunction (impairment versus enhancement) in *Fmr1*$^{-/y}$ mice are both different in the amygdala compared to the hippocampus. As predicted by the mGluR theory, downregulating mGluR signaling corrects multiple FXS-induced abnormalities in the hippocampus and neocortex (Dölen et al., 2007). In contrast, an mGluR-antagonist failed to reverse deficient amygdalar LTP in *Fmr1*$^{-/y}$ mice (Suvrathan et al., 2010). These observations underscore the need to modify the current mGluR-based framework to better explain FXS-related synaptic dysfunction in the amygdala.

How do these divergent patterns of mGluR-plasticity, and their dysfunction in FXS, affect hippocampal versus amygdalar function in the intact animal? Despite extensive analyses of the molecular and synaptic signaling defects in the hippocampus of FXS mice, very few assessed how these alterations lead to specific behavioral abnormalities. For instance, abnormalities in hippocampal mGluR-LTD, and its reversal, have been studied in considerable detail. LTD and mGluR5 expression levels in the hippocampus also modulate spatial learning performance (Kemp and Manahan-Vaughan, 2004; Manahan-Vaughan and Braunewell, 1999, 2005) However, the impact of defects in mGluR-LTD on hippocampal circuit function *in vivo* is not clear and has not yet been linked to specific deficits in learning and memory in mouse models of FXS.

An effective strategy to bridge these gaps comes from rodent models of fear memory, for which the neural circuitry has been characterized extensively across biological scales in the amygdala (Johansen et al., 2011; Maren and Quirk, 2004; Ressler and Maren, 2019; Tovote et al., 2015). Of direct relevance to FXS and mGluR-signaling are findings that mGluR5 in the lateral amygdala plays a pivotal role in fear conditioning and in LTP at synapses involved in fear conditioning (Rodrigues et al., 2002). Further, *in vivo* activation of mGluR5 receptors in the lateral amygdala enhances cue-specific fear, in addition to facilitating LTP *in vitro* (Rahman et al., 2017). Moreover, the gap between the synaptic and behavioral levels can be bridged in a fear conditioning-based framework because recordings in freely behaving animals have shown acquisition of conditioned fear responses to be associated with LTP-like physiological changes *in vivo* in the lateral amygdala (Rogan et al., 1997). An equivalent framework is not available with respect to hippocampal mGluR-LTD. Thus, as a model system, the amygdala offers a way to address several unresolved issues relevant to FXS. For instance, previous findings on synaptic dysfunction caused by FXS were gathered from *in vitro* measurements in amygdalar slices (Suvrathan et al., 2010), however, the functional consequences of these changes, at the circuit and behavioral levels, remain unexplored in the intact animal. At the other end, earlier studies on fear-related behavior have yielded mixed results wherein knockout mice showed either impaired fear recall (Paradee et al., 1999) or no difference compared to normal mice (Dobkin et al., 2000; Hamilton et al., 2014; Peier et al., 2000). Further, *in vivo* electrophysiological analysis of these behaviors has not been attempted in rodent models of FXS. It is also unclear if pharmacological manipulations of mGluRs can correct potential abnormalities in amygdala-dependent conditioned fear and its synaptic correlates. Specifically, would the mGluR theory of FXS also hold in the amygdala despite the divergent patterns of plasticity defects seen in this brain area? The aim of the present study is to address these questions at multiple levels of neural organization in the amygdala of a rat model of FXS. Such analyses in the amygdala are essential for the development of novel strategies to treat the affective symptoms of FXS.

RESULTS

As a first step in our analysis of how FXS disrupts amygdala-dependent behavior, we subjected *Fmr1*$^{-/y}$ rats to auditory fear conditioning, wherein animals rapidly learn to associate a previously neutral tone (conditioned stimulus [CS]) with a coincident aversive stimulus (unconditioned stimulus [US]). Re-exposure to the CS alone evokes a cessation of locomotor activity, or "freezing," which serves as a behavioral measure of the learned association. Accumulating evidence has established that plasticity in the basolateral amygdala (BLA) is essential for encoding fear memories (Blair et al., 2001; Rodrigues et al., 2001; Wilensky et al., 1999). Therefore, we characterized the effects of loss of FMRP on conditioned fear and then examined the underlying *in vivo* and *in vitro* mechanisms at lower levels of neural organization.

Impaired recall of conditioned fear in *Fmr1*$^{-/y}$ rats

Rats chronically implanted with recording electrodes in the BLA first underwent habituation to the context (days 1 and 2) (Figure 1A) and then to the tone that was subsequently used as the CS for repeated pairings with a foot shock (US) (day 3) (Figure 1A). Both wild-type (WT) and *Fmr1*$^{-/y}$ rats showed higher levels of freezing at the end of the CS-US pairings compared to tone habituation (Figure 1B) (unpaired t test, $p < 0.001$) (i.e., they were both capable of learning the tone-shock association). 24 hours later, *Fmr1*$^{-/y}$ animals exhibited significantly lower freezing, compared with WT animals, when presented with only the CS in a different context (testing, day 4) (Figure 1C). Together, these results point to impaired recall of fear memories in *Fmr1*$^{-/y}$ rats.

Impaired potentiation of CS-evoked responses in the BLA of fear conditioned *Fmr1*$^{-/y}$ rats

Next, we examined the neural basis of this memory deficit by recording CS-evoked local field potentials in the BLA of the same freely behaving rats (Figure 1D). Specifically, amplitudes of auditory evoked potentials (AEP), in response to the tone CS, were measured as the difference between the first maxima and first negative peak of the CS-evoked AEP (Figure 1E). During fear recall, AEPs in *Fmr1*$^{-/y}$ rats exhibited a significant reduction in amplitude (Figures 1E and 1F) as well as slope (Figure S1A) compared to WT rats. Because the same animals were used to simultaneously monitor changes in freezing behavior and *in vivo* recordings of AEPs in response to the same presentations of the CS, we also quantified the correlation between the two measures. This analysis revealed a significant positive correlation between the behavioral and electrophysiological responses (Figures 1G and S1B). Notably, WT animals exhibiting robust potentiation of CS-evoked AEPs in the BLA also responded to the CS with higher freezing, thereby clustering in the upper right quadrant of the correlation plot (Figure 1G). On the other hand, data points for the *Fmr1*$^{-/y}$ rats were clustered in the lower left quadrant, indicating deficits in both behavioral and electrophysiological indices of fear recall. Finally, increase in CS-evoked theta power has been identified as a neural correlate of conditioned fear (Likhtik et al., 2014). Consistent with this, BLA theta power (measured as the power of auditory evoked responses in the 2–12 Hz frequency band) exhibited a significant increase in WT rats but not *Fmr1*$^{-/y}$ rats during fear recall (Figures S1C and S1D).

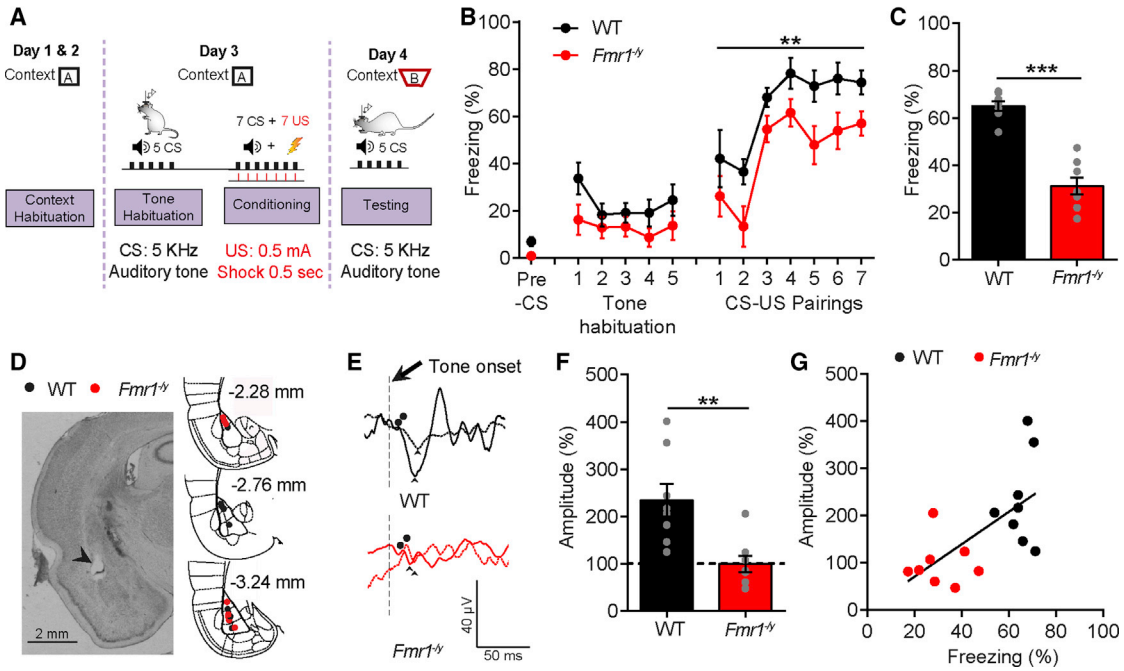

Figure 1. *Fmr1*$^{-/y}$ rats exhibit impaired recall of auditory fear memory and learning-induced enhancement of CS-evoked responses in the BLA

(A) Experimental protocol for auditory fear conditioning. Day 1 and 2, context habituation. Day 3, tone habituation and auditory fear conditioning (CS = 10 s, US = 1 s). Day 4, testing. Auditory evoked potentials (AEPs) were recorded *in vivo* from the BLA in response to all tones during the tone habituation and testing sessions.

(B) There was no difference between the freezing levels of WT and *Fmr1*$^{-/y}$ rats during each of the habituation tones. Unpaired t test, $p > 0.05$. However, although both groups showed an increase in freezing after consecutive CS-US pairings compared to tone habituation (unpaired t test, $p < 0.001$), *Fmr1*$^{-/y}$ rats froze less than WT rats at the end of the pairings. Two-way RM ANOVA, factor: genotype, $F_{(1,14)} = 13.69$, $^{**}p < 0.01$.

(C) *Fmr1*$^{-/y}$ rats showed reduced CS-induced freezing during testing in a different context on day 4. Unpaired t test, $^{***}p < 0.001$.

(D) Representative photomicrograph (left) and schematic coronal sections (right) showing placement of recording electrodes in the BLA.

(E) Representative traces showing AEPs recorded from the BLA in response to the CS during tone habituation (dotted lines) and testing (solid lines). The amplitudes of CS-evoked AEPs were calculated as the difference between the maxima (dot) after the onset of the tone and the negative peak (arrowhead).

(F) Percent change in mean amplitude of AEPs normalized to tone habituation (dotted line). Learning-induced increase in the amplitude of AEPs during testing was seen in WT, but not *Fmr1*$^{-/y}$ rats. Unpaired t test, $^{**}p < 0.01$.

(G) AEP amplitude was positively correlated with the percentage of freezing levels in the same animal during testing of fear memory. Pearson's correlation, $r = 0.64$, $p < 0.01$. WT, N = 8; *Fmr1*$^{-/y}$, N = 8. Data are represented as mean ± SEM.

See also Figure S1.

Deficient LTP and excitatory synaptic transmission in the LA of *Fmr1*$^{-/y}$ *rats*

There is a significant body of evidence that acquisition of fear memory is associated with LTP of synaptic transmission at thalamic inputs to the LA (Bauer et al., 2001; McKernan and Shinnick-Gallagher, 1997; Rogan et al., 1997). Hence, we reasoned that impaired LTP is likely to underlie the deficits seen in our behavioral and *in vivo* analyses in the intact animal. To test this, we compared LTP in principal neurons of the LA using whole-cell current-clamp recordings in coronal brain slices prepared from *Fmr1*$^{-/y}$ and WT rats (Figure 2A). We monitored excitatory postsynaptic potentials (EPSPs) elicited by stimulation of thalamic inputs to LA neurons. Consistent with earlier reports, in brain slices from WT rats, two trains of 100 pulses at 30 Hz resulted in robust LTP. However, the same induction protocol failed to elicit any significant LTP in slices prepared from *Fmr1*$^{-/y}$ rats (Figures 2B and 2C). We next examined the overall status of basal synaptic transmission in these LA neurons by comparing the frequency and amplitude of miniature excitatory postsynaptic currents (mEPSCs) in slices from *Fmr1*$^{-/y}$ and WT rats. *Fmr1*$^{-/y}$ neurons exhibited a significant reduction in mEPSC frequency (Figures 2D and 2E) but not amplitude (Figure S2) compared to WT neurons in the LA, indicating a reduction in basal synaptic transmission.

Reduction in surface GluA1 levels in the BLA of *Fmr1*$^{-/y}$ rats

Next, we probed these impairments in synaptic transmission and plasticity in the BLA at the level of postsynaptic glutamate receptors. Earlier studies have shown that the impact of exaggerated signaling through mGluR5, caused by a loss of the translational repressor FMRP, is manifested in hippocampal area CA1 as enhanced internalization of the AMPAR subunit, GluA1 (Muddashetty et al., 2007; Nakamoto et al., 2007; Snyder et al., 2001). Specifically, this abnormally high GluA1 internalization has been linked to greater mGluR-LTD in the hippocampus. If a similar mechanism is in play in the amygdala, it would disrupt the stabilization of LTP (Figures 2B and 2C). We investigated

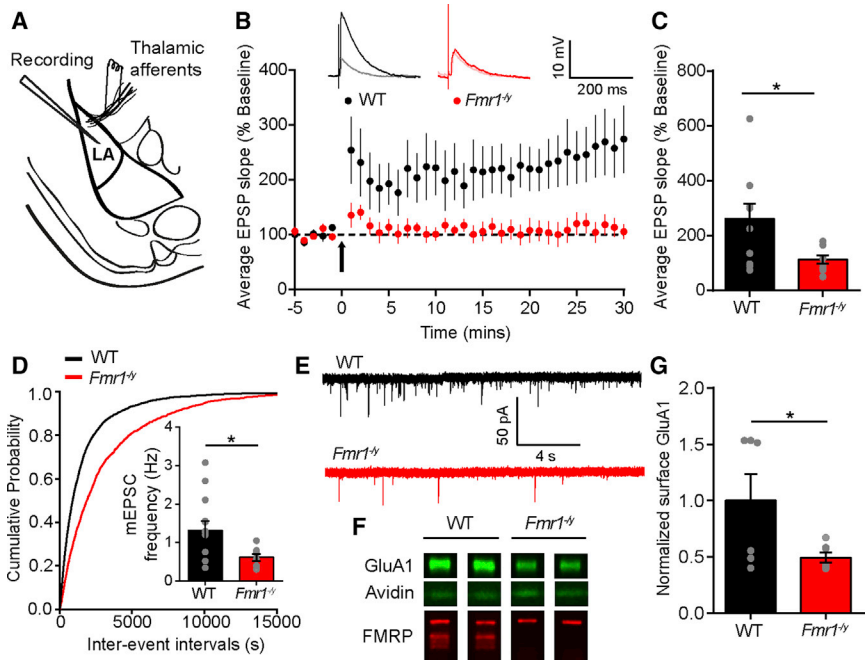

Figure 2. LA neurons in *Fmr1*$^{-/y}$ rats show impaired synaptic transmission and plasticity

(A) Placement of stimulating electrode, activating thalamic afferents, and recording electrodes in the lateral amygdala (LA) in a coronal brain slice.

(B) 30 Hz tetanus (2 trains of 100 pulses, delivered 10 s apart; arrow) induced LTP in principal neurons of slices obtained from WT (n = 10) but not *Fmr1*$^{-/y}$ (n = 9) rats. Two-way RM ANOVA, factor: genotype $F_{(1,17)} = 5.61$, $p < 0.05$. Inset: superimposed representative EPSP traces before (gray, WT; pink, *Fmr1*$^{-/y}$) and after (black, WT; red, *Fmr1*$^{-/y}$) 30-Hz stimulation of thalamic afferents.

(C) Summary of LTP experiments showing normalized EPSP slopes averaged over 25–30 min after tetanic stimulation. LA neurons in *Fmr1*$^{-/y}$ rats exhibited impaired LTP. Unpaired t test, *p < 0.05.

(D) Significantly higher frequency of mEPSCs recorded in LA neurons of WT rats (n = 13) compared to that in *Fmr1*$^{-/y}$ rats (n = 8; unpaired t test, *p < 0.05) as evidenced by a rightward shift in the cumulative probability plot of inter-event intervals (Kolmogorov-Smirnov [KS] test, $p < 0.001$) and reduced mean frequency (inset, unpaired t test, *p < 0.05) in *Fmr1*$^{-/y}$ LA neurons.

(E) Representative mEPSC traces.

(F) Representative western blots showing levels of surface GluA1 normalized to avidin. FMRP was absent in tissue from *Fmr1*$^{-/y}$ rats.

(G) Surface expression of GluA1 in the BLA was reduced in *Fmr1*$^{-/y}$ rats (N = 7) compared to WT rats (N = 6). Unpaired t test, *p < 0.05. Data are represented as mean ± SEM.

See also Figure S2.

this possibility by quantifying levels of biotin-labeled surface GluA1 in BLA slices from *Fmr1*$^{-/y}$ and WT rats. We found a reduction in GluA1 surface expression in *Fmr1*$^{-/y}$ rats (Figures 2F and 2G), which is in agreement with earlier findings in both the amygdala and hippocampus of *Fmr1*$^{-/y}$ mice.

Effects of mGluR-activation on synaptic transmission in the amygdala

The results presented so far identify a range of deficits in amygdalar function in *Fmr1*$^{-/y}$ rats, from impaired fear learning to a reduction in synaptic plasticity and transmission. The mGluR theory of FXS predicts that inhibition of mGluR activity can correct FXS-induced aberrations in the hippocampus (Bear et al., 2004; Dölen et al., 2007). Contrary to this prediction, a previous study found that pharmacological inactivation of mGluR5 with 2-methyl-6-phenylethynyl-pyridine (MPEP) failed to rescue deficient LTP in the LA of *Fmr1*$^{-/y}$ mice (Suvrathan et al., 2010). Perhaps this is not surprising because MPEP is known to block mGluR-dependent LTP (Rodrigues et al., 2002), which was already impaired in the LA of *Fmr1*$^{-/y}$ mice. However, a separate study in rats showed that the opposite manipulation—*in vitro* activation of group 1 mGluRs in the LA using the agonist (RS)-3,5-dihydroxyphenylglycine (DHPG)—caused a robust facilitation of weak LTP, although DHPG by itself did not induce LTP (Rahman et al., 2017). How DHPG achieves its facilitating effects on synaptic transmission in the LA remains unclear.

Studies in the hippocampus reported that DHPG treatment reduces the surface expression of postsynaptic AMPA receptors, a process thought to underlie mGluR-dependent LTD (Fitzjohn et al., 2001; Snyder et al., 2001; Xiao et al., 2001). Hence, we first quantified the impact of bath applied DHPG on the levels of biotin-labeled surface GluA1 in BLA slices (Figure 3A, top). We found a persistent reduction in GluA1 surface expression in slices treated with 50 μM DHPG (Figure 3B). Thus, the reduction in postsynaptic GluA1 surface expression in the amygdala is similar to that reported previously in the hippocampus. Therefore, we reasoned that the difference in the electrophysiological effects on synaptic transmission between the two brain areas is likely to lie on the presynaptic side. Hence, we recorded mEPSCs from the same LA principal neurons before, during, and after bath application of DHPG (Figure 3A, middle). Using this within-cell comparison, we found that the same *in vitro* application of DHPG, despite reducing postsynaptic surface GluA1, increased the frequency of mEPSCs that persisted even after the drug was washed out (Figures 3C and 3D). There was no change in the amplitude of mEPSCs (Figure S3A). Further, DHPG failed to alter the mEPSC frequency in the presence of an mGluR5 antagonist, 3-[(2-methyl-1,3-thiazol-4-yl) ethynyl] pyridine (MTEP) (Figures S3B–S3D), indicating that the increase in frequency was due to DHPG-induced activation of mGluR5. Because this increase in mEPSC frequency is suggestive of changes in presynaptic release probability, we also analyzed the effects of DHPG on paired-pulse facilitation at thalamic inputs to LA neurons. Specifically, we measured paired-pulse ratios (PPR) of evoked EPSCs before, during, and after bath application of DHPG in the same LA neuron (Figure 3A, bottom). This within-cell comparison revealed that DHPG also causes a reduction of PPRs, indicating an increase in presynaptic release

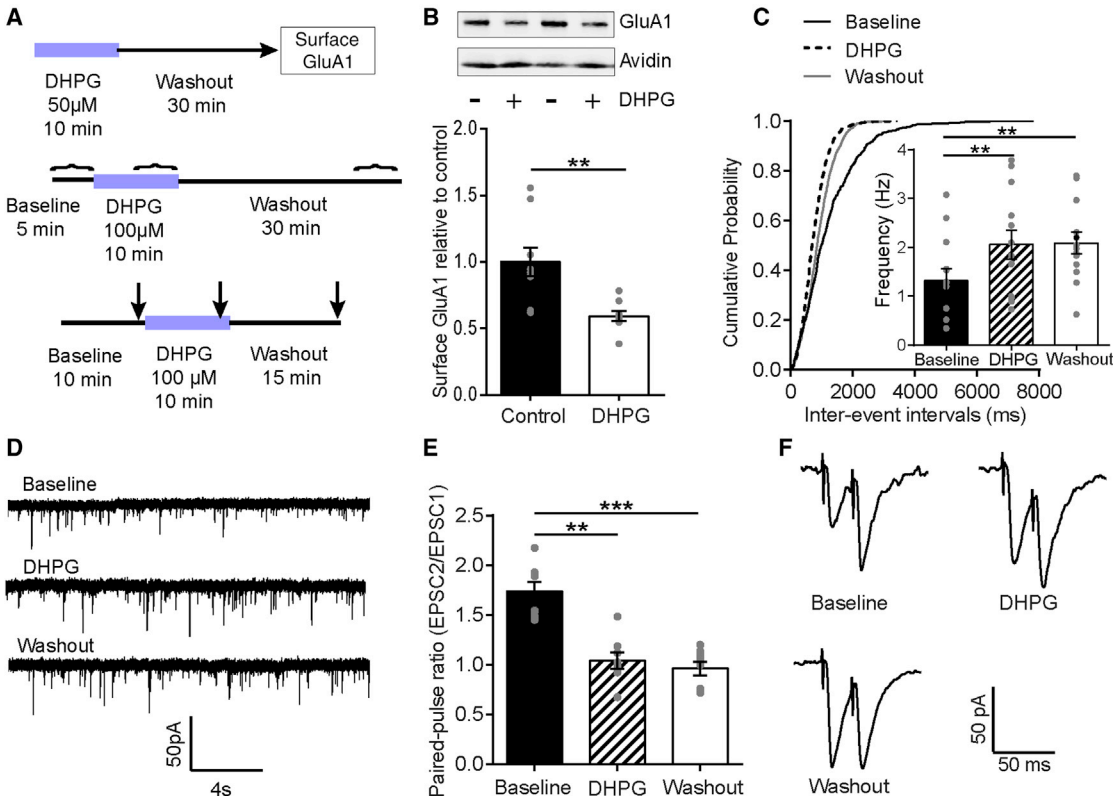

Figure 3. Synaptic effects of DHPG and presynaptic mGluR5 in the LA

(A) Schematic of experimental protocols. Top: the levels of surface GluA1 receptors were measured in BLA slices from control rats after a 10-min bath application of 50 μM DHPG followed by a 30-min washout. Middle: voltage-clamp recordings of mEPSCs were made before (5-min baseline), the last 5 min of 10-min bath application of 100 μM DHPG, and during the last 5 min of a 30-min washout each in the same LA neuron. ( ) Indicates the time points at which mEPSCs were recorded. Bottom: paired-pulse ratios (PPRs) in response to stimulation of thalamic afferents were measured in the same LA neuron before, during, and 15 min after bath application of 100 μM DHPG. (↓) Indicates the time points at which PPRs were monitored.

(B) DHPG induced a reduction in surface GluA1 levels in the BLA. Top: representative western blots showing surface levels of GluA1 normalized to avidin in control and DHPG treated slices. Unpaired t test, $^{**}p < 0.01$. Control, N = 9; DHPG, N = 9.

(C) DHPG increased the frequency of mEPSCs in LA neurons, which remained elevated 30 min after washout. One-way RM ANOVA, $F_{(1,18)} = 7.59$, Bonferroni's test $^{**}p < 0.01$. There was a significant leftward shift in the cumulative probability histogram of inter-event intervals during DHPG application, as well as washout, compared to baseline. KS test, $^{**}p < 0.01$, n = 12.

(D) Representative mEPSC traces before (baseline), during (DHPG) and after washout of DHPG.

(E) Bath application of 100 μM DHPG decreases PPRs recorded in LA neurons. One-way RM ANOVA, $F_{(1,9)} = 38$, Bonferroni's test $^{***}p < 0.001$, n = 8.

(F) Sample of averaged EPSC traces at 25-ms inter-stimulus intervals before, during, and after DHPG application. Data are represented as mean ± SEM.

See also Figure S3.

probability (Figures 3E and 3F). Together, these results suggest that although DHPG strengthens the presynaptic component of transmission in LA neurons, it has the opposite effect on the postsynaptic side.

Presynaptic mGluR5 in the amygdala

Postsynaptic mechanisms of mGluR signaling and plasticity have received greater attention in published analyses of FXS-induced changes in hippocampal area CA1. Analyses using a mouse model of FXS revealed lower presynaptic release as evidenced by a decrease in the frequency mEPSCs, increased PPR, and slower use-dependent block of NMDA receptor currents in the LA (Suvrathan et al., 2010). Further, *in vitro* mGluR-activation using DHPG enhances presynaptic release (Figure 3), which is also consistent with previous findings (Rahman et al., 2017). However, an earlier study on mGluR-dependent plasticity and fear learning, using light and electron microscopy, found that mGluR5 is predominantly located in postsynaptic structures in the LA (Rodrigues et al., 2002). To reconcile the different loci of mGluR action, we examined the localization of mGluR5 in the amygdala and hippocampus. To assess the distribution of mGluR5 relative to the pre- and postsynaptic compartment with high spatial resolution, we used super-resolution protein retention expansion microscopy together with immunocytochemistry (Tillberg et al., 2016). With an increased resolution (of up to ~4×), expansion microscopy allowed us to better measure and quantify mGluR5 localization to either the pre- or postsynaptic compartment (Chien et al., 2015; Hafner et al., 2019). We examined the localization of mGluR5 relative to pre- and postsynaptic terminal markers, RIM1 (Kaeser

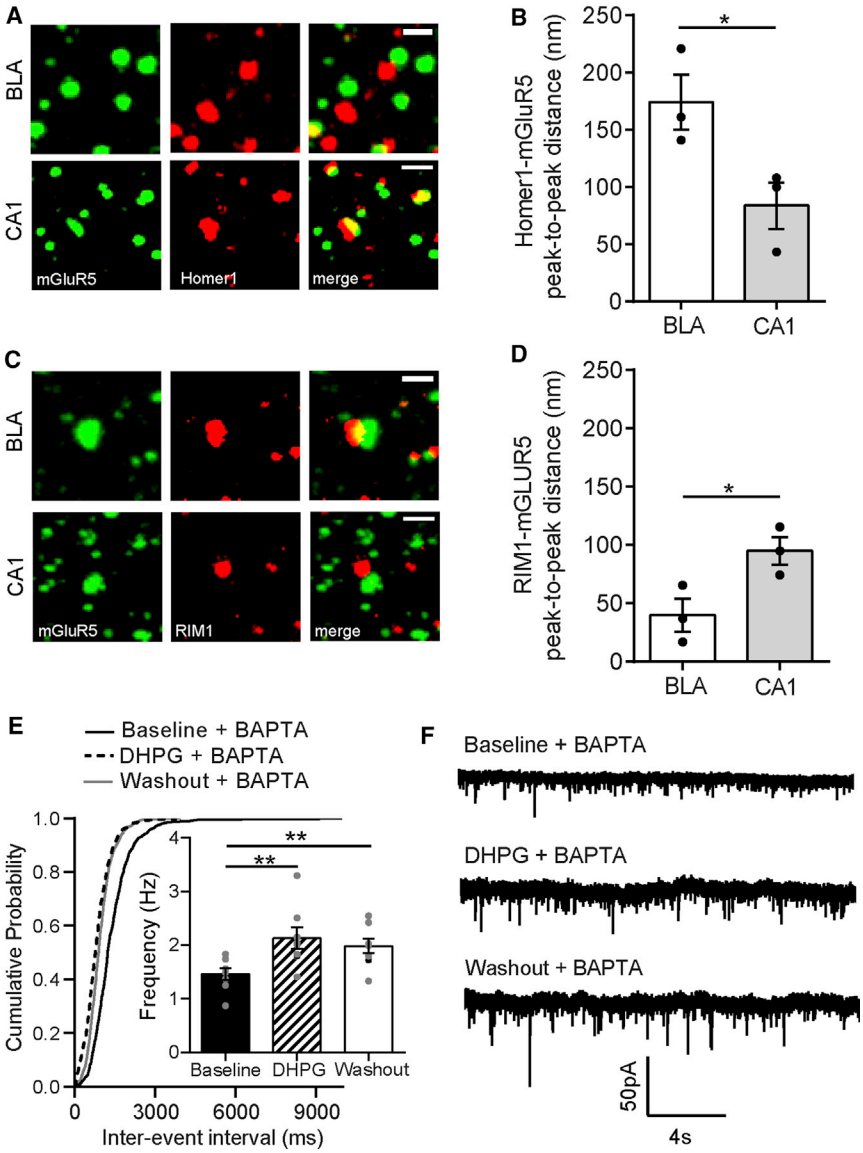

Figure 4. Presynaptic mGluR5 in the LA

(A) Representative images of the BLA (top) and the CA1 region of the hippocampus (bottom) in WT rats showing localization and overlap of mGluR5 (green) and Homer1 (red, postsynaptic marker). Scale bar, 2 μm.

(B) Homer1 and mGluR5 had a greater peak-to-peak distance in the BLA compared to the CA1. Unpaired t test, *$p < 0.05$. N = 3 experiments.

(C) Representative images of the BLA (top) and the CA1 region of the hippocampus (bottom) showing localization and overlap of mGluR5 (green) and RIM1 (red, presynaptic marker). Scale bar, 2 μm.

(D) RIM1 and mGluR5 had a shorter peak-to-peak distance in the BLA compared to the CA1. Unpaired t test, *$p < 0.05$. N = 3 experiments.

(E) DHPG increased mEPSC frequency in LA neurons even after chelating intracellular Ca^{2+} using 10 mM BAPTA. One-way RM ANOVA, $F_{(1,12)} = 9.95$, Bonferroni's test **$p < 0.01$. n = 8. Bath application of DHPG causes a significant leftward shift in in the cumulative probability histogram of inter-event intervals compared to baseline, and this persists after washout. KS test, $p < 0.05$.

(F) Representative mEPSC traces. Data are represented as mean ± SEM.

See also Figure S4.

et al., 2011) and Homer1 (Ehrengruber et al., 2004), in the BLA (Figures 4A and 4C, top) and CA1 region of the hippocampus (Figures 4A and 4C, bottom). We assessed the signal distribution of mGluR5 relative to the pre- and postsynapse, by calculating the peak-signal to peak-signal distance of the immunolabeled puncta for mGluR5 and RIM1 or Homer1 in both the BLA and CA1 (see STAR Methods). We found that mGluR5 was positioned closer to the postsynaptic protein Homer1 in the CA1 area compared to the BLA (Figure 4B). In contrast, mGluR5 was localized closer to the presynaptic protein RIM1 in the BLA than in CA1 (Figure 4D). Taken together, these data indicate a predominantly presynaptic localization for mGluR5 in the BLA.

The analysis in the BLA using expansion microscopy reveals the presence of presynaptic mGluR5 in the BLA. If this is indeed adequate for DHPG to enhance mEPSC frequency, then disrupting the signaling cascade triggered by postsynaptic mGluR5 in the recorded neuron should not diminish the presynaptic effects of DHPG manifested as electrophysiological changes in mEPSC frequency. To test this, we added the Ca^{2+}-chelator, 1,2-bis(2-aminophenoxy) ethane-*N*,*N*,*N*′,*N*′-tetraacetic acid (10 mM BAPTA) in the pipette solution while recording the effects of bath-applied DHPG on LA mEPSCs (using the same protocol depicted in Figure 3A, middle). Strikingly, this manipulation did not prevent the DHPG-induced enhancement in mEPSC frequency in the LA (Figures 4E, 4F, and S4). This argues strongly for a presynaptic mechanism of action for DHPG in enhancing synaptic transmission in the LA.

mGluR-activation corrects deficient synaptic transmission and LTP in the LA

Taken together, these results suggest that activation of mGluRs using DHPG may be well suited to reverse the range of amygdalar deficits we have identified in the *Fmr1*$^{-/y}$ rats. We tested this at three different levels of neural organization (Figures 5 and 6). First, because DHPG enhances mEPSC frequency and the same measure of basal synaptic transmission is suppressed in LA neurons of *Fmr1*$^{-/y}$ rats (Figures 2D and 2E), we examined the effects of mGluR-activation in LA slices prepared from *Fmr1*$^{-/y}$ rats. To this end, we recorded mEPSCs from LA principal neurons before, during, and after bath application of 100 μM DHPG (using the same protocol depicted in Figure 3A, middle). This within-cell comparison revealed that 100 μM

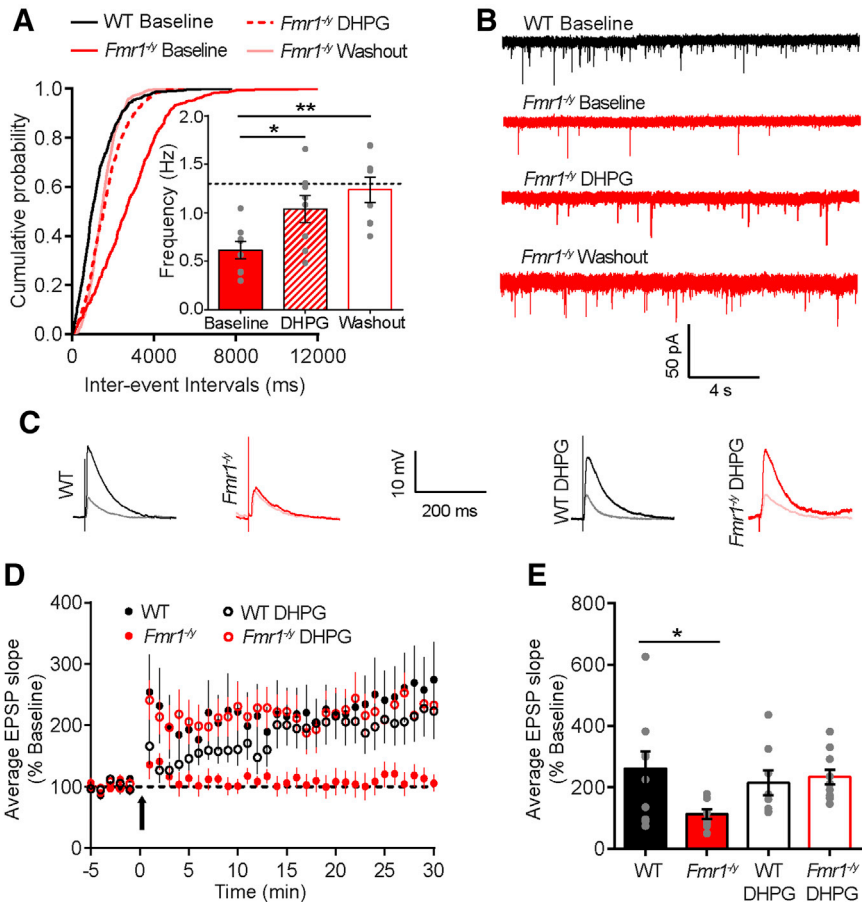

Figure 5. *In vitro* mGluR-activation corrects deficits in synaptic transmission and plasticity in the LA of *Fmr1*$^{-/y}$ rats

(A) Bath application of 100 μM DHPG reversed the decrease in mEPSC frequency in LA neurons of *Fmr1*$^{-/y}$ rats. DHPG application increased mEPSC frequency in *Fmr1*$^{-/y}$ neurons back to WT levels (dotted line), which persisted until the end of the 30-min washout. One-way RM ANOVA, $F_{(1,12)} = 14$, Bonferroni's test *p < 0.05, **p < 0.01. The cumulative frequency histogram of inter-event intervals showed a leftward shift during DHPG application and washout, overlapping with baseline levels of WT neurons. KS test, **p < 0.01. WT, n = 12; *Fmr1*$^{-/y}$, n = 8.

(B) Representative mEPSC traces.

(C) Representative EPSP traces before (gray, WT; pink, *Fmr1*$^{-/y}$) the 30-Hz tetanus and up to 30 min after (black, WT; red, *Fmr1*$^{-/y}$).

(D) High-frequency 30 Hz stimulation (arrow) did not induce LTP in LA neurons from *Fmr1*$^{-/y}$ rats. However, after pre-incubation with DHPG, the same 30-Hz tetanus induced robust LTP in *Fmr1*$^{-/y}$ neurons. Two-way RM ANOVA, factor: DHPG $F_{(1,15)} = 6.12$, *p < 0.05.

(E) Mean values of LTP from minutes 25 to 30, normalized to the 5-min pre-tetanus baseline. DHPG incubation reversed impaired LTP in *Fmr1*$^{-/y}$ LA neurons, causing no further increase in WT LTP. Two-way ANOVA factor: interaction $F_{(1,33)} = 4.92$, *p < 0.05. Tukey's test, *p < 0.05. WT, n = 10; *Fmr1*$^{-/y}$, n = 9; WT DHPG, n = 8; *Fmr1*$^{-/y}$ DHPG, n = 10. Data are represented as mean ± SEM.

See also Figure S5.

DHPG causes a significant increase in mEPSC frequency in *Fmr1*$^{-/y}$ neurons that reached levels comparable to baseline transmission in WT neurons (Figure 5A). This enhancement persisted even 30 min after DHPG was washed out (Figures 5A and 5B). As in the case of WT neurons, DHPG did not change the amplitude of mEPSCs in LA neurons from *Fmr1*$^{-/y}$ rats (Figure S5). Next, we examined the effects of DHPG bath application on LTP in LA slices applying the same induction protocol used earlier (Figures 2A and 2B). After incubation with 100 μM DHPG, tetanic stimulation of thalamic inputs to LA principal neurons triggered robust LTP in *Fmr1*$^{-/y}$ slices, which was significantly greater than the impaired LTP seen in *Fmr1*$^{-/y}$ LA neurons in the absence of DHPG (Figures 5C–5E). Thus, mGluR-activation also reversed the deficient LTP in amygdalar slices from *Fmr1*$^{-/y}$ rats.

mGluR-activation in the amygdala also restores normal fear learning in *Fmr1*$^{-/y}$ rats

What are the behavioral consequences of these synaptic changes induced by mGluR-activation? Specifically, will the reversal of the deficits in basal synaptic transmission and LTP in the LA also restore recall of conditioned fear in the intact *Fmr1*$^{-/y}$ rat? To address this question, we combined the same fear conditioning procedure used earlier (Figure 1A) with targeted *in vivo* infusion of saline or DHPG directly into the BLA of freely behaving *Fmr1*$^{-/y}$ and WT rats (Figure 6A, top). Following context habituation, animals were subjected to bilateral *in vivo* infusions of saline into the BLA and 30 min later underwent habituation to the CS that was subsequently used for auditory conditioning (Figure 6A, bottom). 24 h later, this conditioning led to a significant increase in the freezing response to the CS (Figure 6B) in WT rats (i.e., robust recall of conditioned fear). However, the same conditioning was unable to produce any detectable change in CS-induced freezing in the saline-infused *Fmr1*$^{-/y}$ rats 24 h later (Figure 6B), thereby demonstrating an impairment in fear recall similar to that presented earlier in Figure 1. Next, a separate group of *Fmr1*$^{-/y}$ and WT animals received *in vivo* infusions of DHPG into the BLA, followed by the same sequence of tone habituation and auditory conditioning (Figure 6A, top). In contrast to saline, infusions of DHPG caused higher freezing in both control and *Fmr1*$^{-/y}$ animals before the onset of the first tone (pre-CS) (day 1) (Figure 6A), as well as during subsequent tone habituation (Figure 6A). A day later, however, these animals did not exhibit enhanced pre-CS freezing in the testing context (Figure S6A) but only a selective increase in freezing to the CS (testing, day 2) (Figure 6B). Notably, the levels of CS-induced freezing during the testing session were indistinguishable between the DHPG-treated *Fmr1*$^{-/y}$ and WT rats (Figure 6B). Thus, auditory conditioning, in conjunction with simultaneous *in vivo* activation of mGluR in the BLA, restored normal recall of fear memory in *Fmr1*$^{-/y}$ rats.

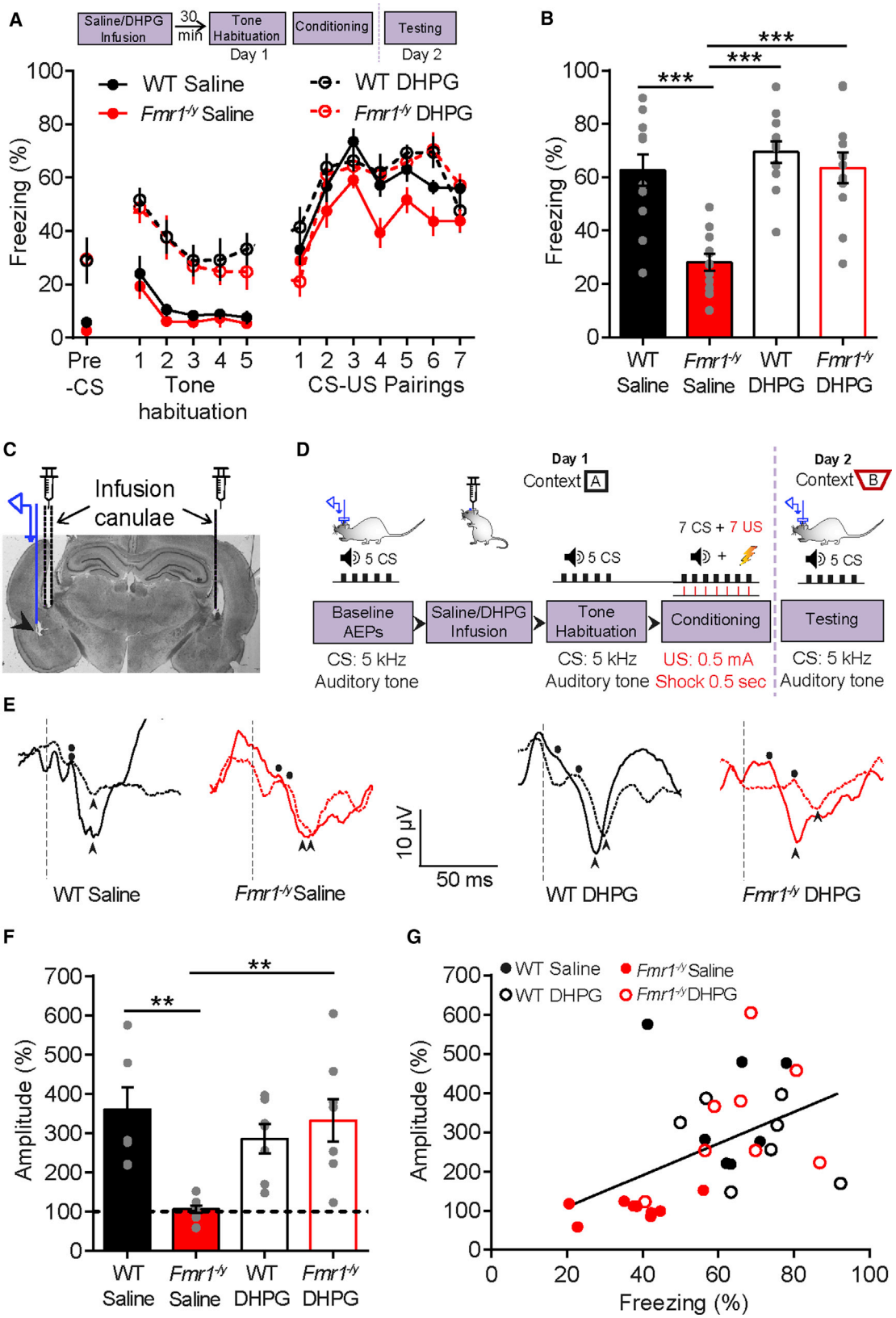

(legend on next page)

In vivo activation of mGluRs in the BLA restores learning-induced increase in behavioral and *in vivo* electrophysiological responses to the CS in *Fmr1*$^{-/y}$ rats

These results demonstrating reversal of amygdalar deficits in FXS rats, using *in vitro* and *in vivo* DHPG treatment, were gathered from separate measurements across levels of neural organization. The DHPG-induced corrections achieved at the level of synaptic plasticity and fear memory recall are consistent with each other, suggesting a link between them. To strengthen this link further, we attempted to integrate these different measures with DHPG infusion into a single experiment. To this end, we monitored if DHPG infusions into the BLA simultaneously corrected deficient recall of fear memory and its underlying *in vivo* correlate – impaired learning-induced potentiation of CS-responses in the BLA – in the same animal. Here too, we used the same fear conditioning protocol (Figure 6D) with targeted bilateral *in vivo* infusion of saline or DHPG directly into the BLA of freely behaving *Fmr1*$^{-/y}$ and WT rats, while carrying out *in vivo* recordings of the changes in CS-evoked AEPs unilaterally from the BLA (Figures 6C, S6B, and S6C). First, consistent with results shown in Figure 6B, *in vivo* mGluR activation in the BLA once again restored normal recall of conditioned fear in *Fmr1*$^{-/y}$ rats (data not shown). Next, in these same rats, simultaneous recordings of CS-evoked responses in the BLA (Figure 6E) allowed us to compare baseline AEPs (dotted lines) recorded on day 1 before infusion of saline/DHPG with those recorded during testing of fear recall (solid lines) on day 2 in both WT (black) and *Fmr1*$^{-/y}$ (red) rats. In rats receiving saline infusion into the BLA, auditory fear conditioning caused an increase in AEP amplitude in WT, but not *Fmr1*$^{-/y}$, rats (Figure 6F). In striking contrast, in conditioned *Fmr1*$^{-/y}$ rats receiving DHPG infusions in the BLA, learning-induced potentiation of CS-evoked AEPs was restored (Figure 6F). Thus, in conditioned *Fmr1*$^{-/y}$ rats receiving DHPG infusions in the BLA, the deficient potentiation of CS-evoked responses in the BLA was prevented, allowing normal recall of fear memory. The deficit in learning-induced increase in theta power, seen in *Fmr1*$^{-/y}$ rats, was not fully restored by DHPG infusion into the BLA (Figures S6D and S6E). Finally, if learning-induced potentiation of CS responses in the BLA is indeed the substrate underlying normal conditioned fear seen, a comparison of the AEP amplitudes measured in individual animals with the freezing levels exhibited by them should reflect a correlation. Indeed, behavioral and *in vivo* electrophysiological data obtained from rats in all four experimental groups displayed a positive correlation between the mean percentage change in CS-evoked AEPs and percentage freezing (Figure 6G), supporting a role for learning-induced enhancement in CS responses in the BLA and normal fear recall. Specifically, the groups that exhibited strong potentiation of BLA responses also showed higher freezing to CS (WT-saline, WT-DHPG), thereby clustering in the upper right quadrant of the correlation plot. In contrast, data points for the *Fmr1*$^{-/y}$-saline group were clustered toward the lower left quadrant, indicating deficits in both measures. However, the data points from *Fmr1*$^{-/y}$ rats that received DHPG infusions into the BLA overlapped with those from the WT rats in the upper right quadrant. Thus, the same *in vivo* mGluR-activation that restored normal recall of conditioned fear also reversed its deficient *in vivo* encoding in the BLA in the same animal.

DISCUSSION

Analyses of various abnormalities in synaptic function and molecular signaling in rodent models of FXS have given rise to a powerful framework, including the ‘‘mGluR theory,’’ for identifying molecular targets for therapeutic strategies against FXS. However, the focus of most of these foundational studies was on the hippocampus. Here, we present findings that add a new dimension to our understanding of FXS-induced dysfunction in the amygdala, which remains less explored despite its central role in the emotional symptoms of the disorder. Motivated by differences between the amygdala and hippocampus in mGluR-dependent modulation of synaptic transmission, we addressed two key questions. First, behavioral characterization of a rat model of FXS revealed deficient recall of conditioned fear. This, in turn, led us to examine both *in vivo* and *in vitro* measures of plasticity underlying fear learning in a specific circuit—the

Figure 6. Targeted *in vivo* mGluR-activation in the BLA restores normal fear learning and its neural correlates in *Fmr1*$^{-/y}$ rats

(A) Inset top: WT and *Fmr1*$^{-/y}$ rats received bilateral *in vivo* infusions (1.0 μL per side) of either saline (0.9% NaCl) or DHPG (50 μM) into the BLA 30 min before tone habituation and were then subjected to auditory fear conditioning (day 1); recall of conditioned fear was tested on day 2. DHPG infusion increased mean freezing levels in both WT and *Fmr1*$^{-/y}$ rats during the pre-CS and tone habituation session. Two-way RM ANOVA factor: DHPG $F_{(5,230)} = 11.04$, ***$p < 0.001$. All 4 groups showed an increase in freezing during subsequent conditioning (7 CS-US pairings: CS = 5 kHz tone, 30 s; US = 0.5 mA foot shock, 1 s).

(B) Although *Fmr1*$^{-/y}$ rats with saline infusion into the BLA showed impaired recall of conditioned fear during testing, DHPG infusion restored normal recall of fear memory. Two-way ANOVA factor: interaction $F_{(1,44)} = 8.77$, **$p < 0.01$. All groups N = 12.

(C) The same saline/ DHPG *in vivo* infusion protocol, using bilateral cannula (dotted lines), was combined with unilateral AEP recordings in the BLA (arrow head) and simultaneous behavioral measurements of freezing.

(D) Experimental protocol for auditory fear conditioning (bottom), combined with in vivo infusion into, and recording from, the BLA (top). Day 1, baseline CS-evoked AEPs were measured before saline/DHPG infusion, followed 30 min later by tone habituation and conditioning (CS = 10 s, US = 1 s, 0.5 mA). Day 2, CS-evoked AEPs were measured again during recall of fear memory (testing).

(E) Representative AEP traces recorded from the BLA during baseline (dotted lines) and during testing (solid lines) on for WT (black) and *Fmr1*$^{-/y}$ (red) rats. The AEP amplitude was calculated as the difference between the maxima (dot) after the onset of the tone and the negative peak (arrowhead).

(F) Percent change in mean amplitude of AEPs normalized to tone habituation (dotted line). A learning-induced increase in the amplitude of AEPs during testing was seen in both WT groups but not *Fmr1*$^{-/y}$ rats receiving saline infusions. In contrast, *Fmr1*$^{-/y}$ rats receiving DHPG infusions show a significant learning-induced enhancement in AEP amplitude during testing. Two-way ANOVA factor: interaction $F_{(1,18)} = 12.64$, $p < 0.01$. Tukey’s test **$p < 0.01$. WT saline, N = 7; *Fmr1*$^{-/y}$ saline, N = 9; WT DHPG, N = 7; *Fmr1*$^{-/y}$ DHPG, N = 8.

(G) AEP amplitude (normalized to tone habituation) was positively correlated with the percentage of freezing levels in the same animal during testing of fear memory. Pearson’s correlation, $r = 0.45$, $p < 0.05$. Data are represented as mean ± SEM.

See also Figure S6.

lateral amygdala (LA)—that is known to mediate this behavior. Enhanced freezing behavior elicited by the tone CS was accompanied by increases in CS-evoked auditory-evoked field potentials in the intact LA of conditioned WT, but not *Fmr1*$^{-/y}$ rats. This deficit was also evident at the synaptic level as impaired LTP in LA principal neurons. Consistent with this LTP deficit, postsynaptic surface expression of the AMPA receptor subunit, GluA1, was reduced in the LA. We also found evidence for reduced presynaptic release in the *Fmr1*$^{-/y}$ rats manifested as a reduction in mEPSC frequency. This presynaptic effect, in turn, served as the starting point for a second line of inquiry—how these deficits associated with FXS may be reversed by targeting mGluRs. Strikingly, in contrast to earlier strategies involving inactivation of mGluR-signaling to correct abnormalities in the hippocampus (Dölen et al., 2007), pharmacological activation of mGluRs reversed the impairment in presynaptic release, as well as LTP, in the LA. mGluR-activation caused a reduction in postsynaptic surface expression of GluA1, suggesting a presynaptic mechanism through which DHPG strengthens synaptic transmission. Consistent with this, our analysis demonstrates the presence of mGluR5 in the presynaptic compartment of LA synapses. We confirmed the functional consequences of activating these presynaptic receptors by showing that DHPG was capable of enhancing mEPSC frequency even when signaling triggered by postsynaptic mGluRs was blocked by chelating Ca^{2+} in the postsynaptic neuron. Upon probing the benefits of this intervention at the behavioral level, we found that *in vivo* mGluR-activation in the BLA of freely behaving *Fmr1*$^{-/y}$ rats reversed deficient fear recall. Finally, this behavioral rescue was accompanied by a simultaneous reversal of the circuit level deficit in the same animal—the impairment of learning-induced enhancement of CS responses was also corrected by *in vivo* mGluR-activation in the amygdala. Together, these results demonstrate the contrasting nature of FXS-induced defects in the amygdala compared to previous findings in the hippocampus. Importantly, this led us to adopt an opposite pharmacological strategy to correct amygdalar aberrations—from synapses through circuit to behavior—in *Fmr1*$^{-/y}$ rats. Thus, group 1 mGluR signaling may still be an effective target for therapeutic interventions against amygdalar defects caused by FXS but in a manner that takes into account circuit-specific differences and presynaptic mechanisms.

Deficient excitatory synaptic transmission and plasticity in the amygdala, and its behavioral manifestation as impaired recall of cue-specific fear, are consistent with accumulating clinical evidence suggesting disruption of appropriate encoding of fear-related information seen in FXS individuals. For example, functional MRI revealed reduced amygdalar activity in affected individuals while viewing fearful facial expressions compared with other stimuli (Kim et al., 2014). Notably, the decrease in amygdala activation in these individuals was fear-specific because this was not seen when participants were viewing happy compared with other types of facial expressions. In men with the *FMR1* premutation, attenuated amygdalar activation has also been seen during an emotion-matching task, as well as impaired startle potentiation while viewing fear faces (Hessl et al., 2011). Consistent with these neuroimaging studies, emotion-potentiated startle, a probe of amygdala activation, was found to be reduced in children and adolescents with FXS compared to a typically developing control group (Ballinger et al., 2014).

In the broader context of earlier findings, our analyses reveal differences, as well as common endpoints, underlying FXS-related synaptic defects in the amygdala and hippocampus. First, we found lower surface GluA1 in BLA slices, similar to that reported in cultured hippocampal neurons (Nakamoto et al., 2007). Second, DHPG application caused a postsynaptic reduction of surface GluA1 in the BLA, which is also similar to what has been seen in hippocampal neurons (Fitzjohn et al., 2001; Snyder et al., 2001; Xiao et al., 2001). Thus, the postsynaptic effects of both FXS and DHPG—reduction of surface GluA1—are similar in the amygdala and hippocampus. However, where the two brain areas appear to differ is on the presynaptic side. Consistent with earlier reports of lower presynaptic release in the LA of a mouse model of FXS (Suvrathan et al., 2010), we report reduced mEPSC frequency in the present study. However, no such reduction in presynaptic release has been observed in hippocampal area CA1 of adult *Fmr1*$^{-/y}$ mice (Braun and Segal, 2000; Pfeiffer and Huber, 2007). In fact, the opposite effect—higher spontaneous EPSC frequencies and lower paired-pulse ratios—have been reported in the hippocampus of younger *Fmr1*$^{-/y}$ mice (Contractor et al., 2015; Tyzio et al., 2014; Klemmer et al., 2011). The most notable difference emerges from the divergent effects of the mGluR-agonist, DHPG, in the two structures. Although DHPG is known to induce LTD in hippocampal area CA1, we show here that it reverses the impairment of LTP in the LA of *Fmr1*$^{-/y}$ rats, despite the baseline reduction in postsynaptic surface AMPARs. Moreover, although an earlier study (Rodrigues et al., 2002) reported postsynaptic localization of mGluR5 in the LA, here we identify presynaptic mGluR5 in the LA, providing a basis for the presynaptic effects of DHPG in the amygdala. The synaptic effects of DHPG in the hippocampus and amygdala are particularly interesting in light of our observations using expansion microscopy, which revealed the existence of both pre- and postsynaptic mGluR5 in these two brain areas. This analysis suggests a greater abundance of presynaptic mGluR5 in the BLA relative to the CA1 area, and more postsynaptic mGluR5 in area CA1 compared to the BLA. Hence, future studies will have to take into account both pre- and postsynaptic effects of mGluR-activation, as well as their brain region-specific variations.

This is also interesting in light of accumulating evidence for the presence of fragile X mental retardation protein (FMRP) in presynaptic or axonal FMRP-containing granules (Akins et al., 2012, 2017; Christie et al., 2009). Specifically, FMRP, which regulates mRNA localization and translation, exhibits distinct brain region-specific patterns of expression in presynaptic compartments and its dysregulation may also contribute to the neurological symptoms of FXS (Akins et al., 2009). This warrants exploring if the levels of presynaptically localized FMRP are different between the LA and the hippocampus. Further, it was recently shown that fear conditioning elicits changes in the translatome in cortical axons that project to the LA (Ostroff et al., 2019). Notably, pathway analysis of the fear learning-induced changes in ribosome-bound mRNAs indicates that FMRP is one of the key upstream regulators of axonal protein synthesis in the LA. In the hippocampus, it is well known that

DHPG stimulates postsynaptic protein synthesis (Raymond et al., 2000; Weiler and Greenough, 1993), which is disrupted in *Fmr1*$^{-/y}$ mice (Bowling et al., 2019; Darnell and Klann, 2013; Hou et al., 2006; Osterweil et al., 2010; Waung and Huber, 2009). Thus, it will be important to determine whether fear conditioning-induced presynaptic protein synthesis in the LA requires mGluR5 and whether it is disrupted in *Fmr1*$^{-/y}$ rats.

Finally, these differences in mGluR-dependent synaptic transmission, and its aberration in FXS, add to growing evidence for brain region-specific, even cell-type-specific, changes induced by the loss of FMRP (Contractor et al., 2015; Wang et al., 2014). This also poses a significant therapeutic challenge because a pharmacological strategy that is effective in one brain area, such as an mGluR5-antagonist in the hippocampus, may need to be modified for another area like the amygdala. Recent failures of clinical trials using mGluR5-antagonists may be indicative of some of these issues related to circuit-specific differences. For example, a randomized, double-blind, placebo-controlled trial using a selective mGluR5-antagonist did not reveal any significant effect on emotional function in FXS patients (Berry-Kravis et al., 2016). Thus, an essential step toward overcoming these challenges requires us to focus on specific behavioral symptoms of FXS and then probe the underlying functional changes at the synaptic and molecular levels within specific circuits underlying those particular behavioral deficits. In the present study, we attempted to achieve this by leveraging the advantages offered by auditory fear conditioning, a well-established model of fear learning for which the underlying neural circuitry has been characterized extensively. This enabled us to systematically probe if perturbations caused by FXS at one level of neural organization are consistent with predicted alterations at another. Findings gathered from such an approach offer a new framework, spanning biological scales, for understanding and modulating activity in a well-defined fear circuit and thereby suggesting strategies for treating affective symptoms associated with FXS.

STAR★METHODS

Detailed methods are provided in the online version of this paper and include the following:

SUPPLEMENTAL INFORMATION

Supplemental information can be found online at https://doi.org/10.1016/j.celrep.2021.109805.

ACKNOWLEDGMENTS

We thank Dr. Aditi Bhattacharya for discussions and advice. We also thank Beatriz Alvarez-Castelao, Teresa Spanò, and Belquis Nassim-Assir for help in the perfusion and slicing for the expansion microscopy experiments and Dr. Rakhi Pal and BioRender.com for help with the illustrations. This work was supported by the Department of Biotechnology, Government of India (BT/MB-CNDS/2013). S.C. and his laboratory are supported by intramural funds from NCBS-TIFR, Department of Atomic Energy, Government of India. We gratefully acknowledge financial support from Simons Foundation Autism Research Initiative (529085 to P.C.K.) and The Patrick Wild Centre (to P.C.K., S.C., and D.J.A.W.). P.K.M. is supported by the Department of Science and Technology, Government of India (DST/CSRI/PDF-22/2018) under Cognitive Science Research Initiative (CSRI). P.G.D.-A. is supported by the Peter and Traudl Engelhard Stiftung and the Alexander von Humboldt Foundation (USA-1198990-HFST-P).

AUTHOR CONTRIBUTIONS

G.F., P.K.M., M.M.R., and S.C. designed the study. G.F., P.K.M., M.S.N., P.G.D.-A., A.H., S.K., A.K., and D.S. conducted the experiments and analyzed data. M.M.R. provided computer code for and assisted in the analysis of *in vivo* electrophysiological data. G.F. and S.C. wrote the paper along with input from all authors.

DECLARATION OF INTERESTS

The authors declare no competing interests.

Received: March 17, 2021
Revised: July 19, 2021
Accepted: September 16, 2021
Published: October 12, 2021

REFERENCES

Akins, M.R., Berk-Rauch, H.E., and Fallon, J.R. (2009). Presynaptic translation: stepping out of the postsynaptic shadow. Front. Neural Circuits *3*, 17.

Akins, M.R., Leblanc, H.F., Stackpole, E.E., Chyung, E., and Fallon, J.R. (2012). Systematic mapping of fragile X granules in the mouse brain reveals a potential role for presynaptic FMRP in sensorimotor functions. J. Comp. Neurol. *520*, 3687–3706.

Akins, M.R., Berk-Rauch, H.E., Kwan, K.Y., Mitchell, M.E., Shepard, K.A., Korsak, L.I.T., Stackpole, E.E., Warner-Schmidt, J.L., Sestan, N., Cameron, H.A., and Fallon, J.R. (2017). Axonal ribosomes and mRNAs associate with fragile X granules in adult rodent and human brains. Hum. Mol. Genet. *26*, 192–209.

Ballinger, E.C., Cordeiro, L., Chavez, A.D., Hagerman, R.J., and Hessl, D. (2014). Emotion potentiated startle in fragile X syndrome. J. Autism Dev. Disord. *44*, 2536–2546.

Bauer, E.P., LeDoux, J.E., and Nader, K. (2001). Fear conditioning and LTP in the lateral amygdala are sensitive to the same stimulus contingencies. Nat. Neurosci. *4*, 687–688.

Bear, M.F., Huber, K.M., and Warren, S.T. (2004). The mGluR theory of fragile X mental retardation. Trends Neurosci. *27*, 370–377.

Berry-Kravis, E., Des Portes, V., Hagerman, R., Jacquemont, S., Charles, P., Visootsak, J., Brinkman, M., Rerat, K., Koumaras, B., Zhu, L., et al. (2016). Mavoglurant in fragile X syndrome: Results of two randomized, double-blind, placebo-controlled trials. Sci. Transl. Med. *8*, 321ra5.

Blair, H.T., Schafe, G.E., Bauer, E.P., Rodrigues, S.M., and LeDoux, J.E. (2001). Synaptic plasticity in the lateral amygdala: a cellular hypothesis of fear conditioning. Learn. Mem. *8*, 229–242.

Bowling, H., Bhattacharya, A., Zhang, G., Alam, D., Lebowitz, J.Z., Bohm-Levine, N., Lin, D., Singha, P., Mamcarz, M., Puckett, R., et al. (2019). Altered steady state and activity-dependent de novo protein expression in fragile X syndrome. Nat. Commun. *10*, 1710.

Braun, K., and Segal, M. (2000). FMRP involvement in formation of synapses among cultured hippocampal neurons. Cereb. Cortex *10*, 1045–1052.

Chien, F., Tillberg, P.W., and Boyden, E.S. (2015). Expansion Microscopy. Science *347*, 543–549.

Christie, S.B., Akins, M.R., Schwob, J.E., and Fallon, J.R. (2009). The FXG: a presynaptic fragile X granule expressed in a subset of developing brain circuits. J. Neurosci. *29*, 1514–1524.

Contractor, A., Klyachko, V.A., and Portera-Cailliau, C. (2015). Altered Neuronal and Circuit Excitability in Fragile X Syndrome. Neuron *87*, 699–715.

Darnell, J.C., and Klann, E. (2013). The translation of translational control by FMRP: therapeutic targets for FXS. Nat. Neurosci. *16*, 1530–1536.

Dobkin, C., Rabe, A., Dumas, R., El Idrissi, A., Haubenstock, H., and Brown, W.T.E.D. (2000). Fmr1 knockout mouse has a distinctive strain-specific learning impairment. Neuroscience *100*, 423–429.

Dölen, G., Osterweil, E., Rao, B.S.S., Smith, G.B., Auerbach, B.D., Chattarji, S., and Bear, M.F. (2007). Correction of fragile X syndrome in mice. Neuron *56*, 955–962.

Ehrengruber, M.U., Kato, A., Inokuchi, K., and Hennou, S. (2004). Homer/Vesl proteins and their roles in CNS neurons. Mol. Neurobiol. *29*, 213–227.

Fitzjohn, S.M., Palmer, M.J., May, J.E.R., Neeson, A., Morris, S.A.C., and Collingridge, G.L. (2001). A characterisation of long-term depression induced by metabotropic glutamate receptor activation in the rat hippocampus in vitro. J. Physiol. *537*, 421–430.

Hafner, A.-S., Donlin-Asp, P.G., Leitch, B., Herzog, E., and Schuman, E.M. (2019). Local protein synthesis is a ubiquitous feature of neuronal pre- and postsynaptic compartments. Science *364*, 1–12.

Hamilton, S.M., Green, J.R., Veeraragavan, S., Yuva, L., McCoy, A., Wu, Y., Warren, J., Little, L., Ji, D., Cui, X., et al. (2014). Fmr1 and Nlgn3 knockout rats: novel tools for investigating autism spectrum disorders. Behav. Neurosci. *128*, 103–109.

Hessl, D., Rivera, S., Koldewyn, K., Cordeiro, L., Adams, J., Tassone, F., Hagerman, P.J., and Hagerman, R.J. (2007). Amygdala dysfunction in men with the fragile X premutation. Brain *130*, 404–416.

Hessl, D., Wang, J.M., Schneider, A., Koldewyn, K., Le, L., Iwahashi, C., Cheung, K., Tassone, F., Hagerman, P.J., and Rivera, S.M. (2011). Decreased fragile X mental retardation protein expression underlies amygdala dysfunction in carriers of the fragile X premutation. Biol. Psychiatry *70*, 859–865.

Hou, L., Antion, M.D., Hu, D., Spencer, C.M., Paylor, R., and Klann, E. (2006). Dynamic translational and proteasomal regulation of fragile X mental retardation protein controls mGluR-dependent long-term depression. Neuron *51*, 441–454.

Huber, K.M., Gallagher, S.M., Warren, S.T., and Bear, M.F. (2002). Altered synaptic plasticity in a mouse model of fragile X mental retardation. Proc. Natl. Acad. Sci. USA *99*, 7746–7750.

Johansen, J.P., Cain, C.K., Ostroff, L.E., and LeDoux, J.E. (2011). Molecular mechanisms of fear learning and memory. Cell *147*, 509–524.

Kaeser, P.S., Deng, L., Wang, Y., Dulubova, I., Liu, X., Rizo, J., and Südhof, T.C. (2011). RIM proteins tether Ca2+ channels to presynaptic active zones via a direct PDZ-domain interaction. Cell *144*, 282–295.

Kemp, A., and Manahan-Vaughan, D. (2004). Hippocampal long-term depression and long-term potentiation encode different aspects of novelty acquisition. Proc. Natl. Acad. Sci. USA *101*, 8192–8197.

Kim, S.Y., Burris, J., Bassal, F., Koldewyn, K., Chattarji, S., Tassone, F., Hessl, D., and Rivera, S.M. (2014). Fear-specific amygdala function in children and adolescents on the fragile x spectrum: a dosage response of the FMR1 gene. Cereb. Cortex *24*, 600–613.

Klemmer, P., Meredith, R.M., Holmgren, C.D., Klychnikov, O.I., Stahl-Zeng, J., Loos, M., van der Schors, R.C., Wortel, J., de Wit, H., Spijker, S., et al. (2011). Proteomics, ultrastructure, and physiology of hippocampal synapses in a fragile X syndrome mouse model reveal presynaptic phenotype. J. Biol. Chem. *286*, 25495–25504.

Likhtik, E., Stujenske, J.M., Topiwala, M.A., Harris, A.Z., and Gordon, J.A. (2014). Prefrontal entrainment of amygdala activity signals safety in learned fear and innate anxiety. Nat. Neurosci. *17*, 106–113.

Manahan-Vaughan, D., and Braunewell, K.-H. (1999). Novelty acquisition is associated with induction of hippocampal long-term depression. Proc. Natl. Acad. Sci. USA *96*, 8739–8744.

Manahan-Vaughan, D., and Braunewell, K.H. (2005). The metabotropic glutamate receptor, mGluR5, is a key determinant of good and bad spatial learning performance and hippocampal synaptic plasticity. Cereb. Cortex *15*, 1703–1713.

Maren, S., and Quirk, G.J. (2004). Neuronal signalling of fear memory. Nat. Rev. Neurosci. *5*, 844–852.

McKernan, M.G., and Shinnick-Gallagher, P. (1997). Fear conditioning induces a lasting potentiation of synaptic currents in vitro. Nature *390*, 607–611.

Muddashetty, R.S., Kelić, S., Gross, C., Xu, M., and Bassell, G.J. (2007). Dysregulated metabotropic glutamate receptor-dependent translation of AMPA receptor and postsynaptic density-95 mRNAs at synapses in a mouse model of fragile X syndrome. J. Neurosci. *27*, 5338–5348.

Nakamoto, M., Nalavadi, V., Epstein, M.P., Narayanan, U., Bassell, G.J., and Warren, S.T. (2007). Fragile X mental retardation protein deficiency leads to excessive mGluR5-dependent internalization of AMPA receptors. Proc. Natl. Acad. Sci. USA *104*, 15537–15542.

Osterweil, E.K., Krueger, D.D., Reinhold, K., and Bear, M.F. (2010). Hypersensitivity to mGluR5 and ERK1/2 leads to excessive protein synthesis in the hippocampus of a mouse model of fragile X syndrome. J. Neurosci. *30*, 15616–15627.

Ostroff, L.E., Santini, E., Sears, R., Deane, Z., Kanadia, R.N., LeDoux, J.E., Lhakhang, T., Tsirigos, A., Heguy, A., and Klann, E. (2019). Axon TRAP reveals learning-associated alterations in cortical axonal mRNAs in the lateral amygdala. eLife *8*, 1–24.

Palmer, M.J., Irving, A.J., Seabrook, G.R., Jane, D.E., and Collingridge, G.L. (1997). The group I mGlu receptor agonist DHPG induces a novel form of LTD in the CA1 region of the hippocampus. Neuropharmacology *36*, 1517–1532.

Paradee, W., Melikian, H.E., Rasmussen, D.L., Kenneson, A., Conn, P.J., and Warren, S.T. (1999). Fragile X mouse: strain effects of knockout phenotype and evidence suggesting deficient amygdala function. Neuroscience *94*, 185–192.

Peier, A.M., McIlwain, K.L., Kenneson, A., Warren, S.T., Paylor, R., and Nelson, D.L. (2000). (Over)correction of FMR1 deficiency with YAC transgenics: behavioral and physical features. Hum. Mol. Genet. *9*, 1145–1159.

Pfeiffer, B.E., and Huber, K.M. (2007). Fragile X mental retardation protein induces synapse loss through acute postsynaptic translational regulation. J. Neurosci. *27*, 3120–3130.

Rahman, M.M., Kedia, S., Fernandes, G., and Chattarji, S. (2017). Activation of the same mGluR5 receptors in the amygdala causes divergent effects on specific versus indiscriminate fear. eLife *6*, e25665.

Raymond, C.R., Thompson, V.L., Tate, W.P., and Abraham, W.C. (2000). Metabotropic glutamate receptors trigger homosynaptic protein synthesis to prolong long-term potentiation. J. Neurosci. *20*, 969–976.

Ressler, R.L., and Maren, S. (2019). Synaptic encoding of fear memories in the amygdala. Curr. Opin. Neurobiol. *54*, 54–59.

Rodrigues, S.M., Schafe, G.E., and LeDoux, J.E. (2001). Intra-amygdala blockade of the NR2B subunit of the NMDA receptor disrupts the acquisition but not the expression of fear conditioning. J. Neurosci. *21*, 6889–6896.

Rodrigues, S.M., Bauer, E.P., Farb, C.R., Schafe, G.E., and LeDoux, J.E. (2002). The group I metabotropic glutamate receptor mGluR5 is required for fear memory formation and long-term potentiation in the lateral amygdala. J. Neurosci. *22*, 5219–5229.

Rogan, M.T., Stäubli, U.V., and LeDoux, J.E. (1997). Fear conditioning induces associative long-term potentiation in the amygdala. Nature *390*, 604–607.

Snyder, E.M., Philpot, B.D., Huber, K.M., Dong, X., Fallon, J.R., and Bear, M.F. (2001). Internalization of ionotropic glutamate receptors in response to mGluR activation. Nat. Neurosci. *4*, 1079–1085.

Suvrathan, A., Hoeffer, C.A., Wong, H., Klann, E., and Chattarji, S. (2010). Characterization and reversal of synaptic defects in the amygdala in a mouse model of fragile X syndrome. Proc. Natl. Acad. Sci. USA *107*, 11591–11596.

Till, S.M., Asiminas, A., Jackson, A.D., Katsanevaki, D., Barnes, S.A., Osterweil, E.K., Bear, M.F., Chattarji, S., Wood, E.R., Wyllie, D.J.A., and Kind, P.C. (2015). Conserved hippocampal cellular pathophysiology but distinct behavioural deficits in a new rat model of FXS. Hum. Mol. Genet. *24*, 5977–5984.

Tillberg, P.W., Chen, F., Piatkevich, K.D., Zhao, Y., Yu, C.C., English, B.P., Gao, L., Martorell, A., Suk, H.J., Yoshida, F., et al. (2016). Protein-retention expansion microscopy of cells and tissues labeled using standard fluorescent proteins and antibodies. Nat. Biotechnol. *34*, 987–992.

Tovote, P., Fadok, J.P., and Lüthi, A. (2015). Neuronal circuits for fear and anxiety. Nat. Rev. Neurosci. *16*, 317–331.

Tyzio, R., Nardou, R., Ferrari, D.C., Tsintsadze, T., Shahrokhi, A., Eftekhari, S., Kalilov, I., Tsintsadze, V., Brouchoud, C., Chazal, G., et al. (2014). Oxytocin-Mediated GABA Inhibition During Delivery Attenuates Autism Pathogenesis in Rodent Offspring. Science *343*, 675–680.

Wang, G.X., Smith, S.J., and Mourrain, P. (2014). Fmr1 KO and fenobam treatment differentially impact distinct synapse populations of mouse neocortex. Neuron *84*, 1273–1286.

Waung, M.W., and Huber, K.M. (2009). Protein translation in synaptic plasticity: mGluR-LTD, Fragile X. Curr. Opin. Neurobiol. *19*, 319–326.

Weiler, I.J., and Greenough, W.T. (1993). Metabotropic glutamate receptors trigger postsynaptic protein synthesis. Proc. Natl. Acad. Sci. USA *90*, 7168–7171.

Wilensky, A.E., Schafe, G.E., and LeDoux, J.E. (1999). Functional inactivation of the amygdala before but not after auditory fear conditioning prevents memory formation. J. Neurosci *19*, RC48.

Xiao, M.Y., Zhou, Q., and Nicoll, R.A. (2001). Metabotropic glutamate receptor activation causes a rapid redistribution of AMPA receptors. Neuropharmacology *41*, 664–671.

STAR★METHODS

KEY RESOURCES TABLE

REAGENT or RESOURCE	SOURCE	IDENTIFIER
Antibodies		
anti- GluR1 NT, mouse monoclonal	Millipore, MAB2263,	RRID:AB_11212678
anti- avidin, mouse monoclonal	Invitrogen, MA1-21418	RRID:AB_557672
anti- RIM1, guinea pig polyclonal	Synaptic Systems, 140005	RRID:AB_2661872
anti- Homer, guinea pig polyclonal	Synaptic Systems, 160004	RRID:AB_10549720
anti- mGluR5, rabbit polyclonal	Neuromics, RA16100	RRID:AB_1619239
IR dye 680RD anti-Rabbit IgG	Li-COR Biotechnology	Cat# - P/N 926-68071
IR dye 800CW anti-mouse IgG	Li-COR Biotechnology	Cat# - P/N 926-32210
Chemicals, peptides, and recombinant proteins		
(S) 3,5-Dihydroxyphenylglycine (DHPG)	Abcam	Cat# - Ab120007
EZ-Link^{TM} Sulpho- NHS-SS-Biotin	Thermo Fisher	Cat# - 21331
Pierce Neutravidin agarose	Thermo Fisher	Cat# - 29200
Experimental Models: Organisms/Strains		
Rat: *Fmr1*$^{-/y}$, Sprague Dawley	Sage Labs (now part of Horizon Discovery)	
Deposited data		
Code used in data analysis	This paper	https://zenodo.org/record/5502814

RESOURCE AVAILABILITY

Lead contact

Further information and requests for resources and reagents should be directed to and will be fulfilled by the corresponding author, Dr. Sumantra Chattarji (shona@ncbs.res.in).

Materials availability

This study did not generate new unique reagents or biological samples.

Data and code availability

All data reported in this paper is available from the Lead Contact upon request.

All original code has been deposited at Zenodo and is publicly available as of the date of publication. The DOI is listed in the Key resources table.

Any additional information required to reanalyze the data reported in this work is available from the Lead Contact upon request.

EXPERIMENTAL MODEL AND SUBJECT DETAILS

Male *Fmr1*$^{-/y}$ Sprague Dawley rats and their wild-type (WT) littermate controls (8-10 weeks old, 300-350 g) were obtained from Sigma Advanced Genetic Engineering (SAGE) Labs (St. Louis, MO, USA) and maintained on a 14-h/10-h light/dark cycle with food and water provided *ad libitum*. All experimental subjects were group housed (2-5 animals/cage) to avoid the effects of isolation and randomly assigned to experimental groups. Experiments were done blind to genotype. Rats were handled for 2-3 days to habituate them to the experimenter before the start of each experiment. All experiments were conducted in accordance with the guidelines of the CPCSEA, Government of India and approved by the Institutional Animal Ethics Committees of the National Centre for Biological Sciences and the Institute for Stem Cell and Regenerative Medicine.

METHOD DETAILS

Behavioral protocols

Fear conditioning and fear memory recall tests were performed in different contexts located inside sound-isolation boxes (Coulbourn Instruments, Whitehall, PA, USA). Foot-shocks (US) were delivered through metal grids on the floor (context A: 12 inches wide x 10

inches deep x 12 inches high, no odor), while testing was done in a modified home cage (Context B: 14 inches wide x 8 inches deep x 16 inches high, mint odor). Lighting conditions, floors, and walls were different for each context. All chambers were cleaned with 70% alcohol before each experiment. Infrared LED cues, positioned on the walls of the chambers, were triggered in coincidence with auditory stimuli to monitor the tone-evoked freezing response offline. During context habituation (Days 1&2) (Figure 1A), the rats were allowed to explore context A for 25 minutes each, on 2 consecutive days. During tone habituation (Day 3), the rats received five presentations of an auditory tone (5 kHz, 30 s tone consisting of 30 pips of 100 ms duration at a frequency of 1 Hz; 5 ms rise and fall, 70 ± 5 dB sound pressure level) in context A. This was immediately followed by the fear conditioning protocol, where the tone (CS) was paired (7 pairings, average inter-trial interval < ITI > = 120 s, with a range of 80–160 s) with a co-terminating 0.5 s scrambled foot shock (US; 0.5 mA). In the testing session (Day 4), the rats were introduced into context B and presented with the same tone (CS) to test recall of fear memory. Behavioral recordings were made using a video camera fixed to the wall of the sound isolation box and a frame grabber (sampling at 30 Hz). The videos were stored offline for further manual quantification of freezing behavior by a blind experimenter. Freezing was defined as the absence of movement except due to respiration. In addition to the time spent freezing to the tones, freezing levels were measured for a 10 s period (pre-CS) immediately before the start of the tone trials for every session to assess context-dependent fear. In experiments with targeted bilateral infusions (Figure 6), saline or DHPG was infused into the BLA 30 min before tone habituation. In experiments with both infusions and AEP recordings (Figures 6C–6G), a baseline was included immediately before the infusion of saline or DHPG.

Surgical procedures and *in vivo* extracellular recordings

Rats were subjected to anesthesia with 5% isoflurane and then sustained in anesthesia with 1.5%–2% isoflurane. The level of anesthesia was frequently monitored throughout the procedure using the pedal withdrawal reflex to toe pinch and body temperature maintained with a heating pad. Burr holes were drilled at the stereotaxic co-ordinates of the BLA (3.3 mm posterior to bregma and ± 5.3 mm lateral to midline) and a bundle of 4 formavar-insulated stainless steel electrodes (50 μm diameter; AM Systems, Carlsborg, WA, USA) were implanted using the stereotaxic frame (8.3 mm ventral from the brain surface). The implant was secured using anchor screws and dental acrylic cement. One of the anchor screws was connected to the ground electrode. Similar surgical procedures were used during bilateral implantation of stainless-steel cannulae (Figures 6 and S6) for targeted infusion of DHPG into the BLA. Guide cannulae were implanted using the stereotaxic frame (7.0 mm ventral from the brain surface) and dummy cannulae (28 gauge, with a 0.5 mm projection) were inserted into them to prevent clogging. In experiments with both infusion and AEP recordings (Figures 6 and S6), bundled electrodes (as described above) were attached to one of the guide cannulae and implanted unilaterally. Rats were permitted to recover for 7-10 days following surgery. In the post-surgery period, the rats were singly housed in separate cages. AEPs were recorded using a unit gain buffer head stage (HS-36-Flex; Neuralynx, Bozeman, MT, USA) and the Digilynx data acquisition system (Neuralynx). Signals were amplified (1000X) and acquired at a sampling rate of 1 kHz followed by a band-pass filter (1-500 Hz) using Cheetah data acquisition software (Neuralynx).

Data analysis

AEPs -

The recorded AEPs were averaged over all the tone pips for the specified trial blocks. Averaged AEPs were quantified by measuring the amplitude and slope as the difference between the maxima after the onset of the response and the negative peak. AEP amplitudes and slopes were calculated during tone habituation and testing of fear memory. All AEP amplitudes and slopes were normalized as a percentage of the value during tone habituation (Figure 1) or pre-infusion baseline (Figures 6C–6G) for each animal.

Time-frequency analysis -

Event related variations in spectral power were calculated by time-frequency analysis executed using continuous wavelet transformation (MATLAB, MathWorks Inc., Natick, MA, USA) on the averaged AEPs. Complex Morlet wavelets were used to compute the phase and amplitude of evoked responses within a frequency range from 2 to 100 Hz in steps of 0.1 Hz. The bandwidth parameter and center frequency of the mother wavelet were 2 and 1 Hz respectively. Subsequently, the wavelet power of the time series was calculated and expressed in decibels. Baseline average power for the duration of 0 to −200 ms was subtracted across all time points for each frequency bands. Tone evoked theta power was computed over the duration of 0 to 250 ms from tone onset for frequencies from 2 to 12 Hz.

Targeted pharmacological infusion of DHPG into the BLA

Bilateral infusion of DHPG in the BLA was done using standard pressure injection methods (Rahman et al., 2017). During the infusion procedure, the rats were retained in their home cages and an injection cannula with 1 mm projection (28 gauge, Plastic One, Roanoke, VA, USA) were inserted through the guide-cannula. Using polyethylene tubing, the injection cannula was connected to a Hamilton syringe (10 μl), mounted on an infusion pump (Harvard Apparatus, Holliston, MA, USA). Either vehicle (0.9% (vol/vol) NaCl (1.0 μl per side) or DHPG (1.0 μl per side, 50 μM in saline; Ab120007 Abcam, Cambridge, UK) was infused at a rate of 0.2 μl min^{-1}. The injection cannula was held in place for 5 min after the end of infusion, to permit the drug to diffuse into the tissue.

Histology

After the experiment was completed, rats were deeply anesthetized (ketamine/xylazine, 100/20 mg per kg) and electrolytic lesions (20 μA, 20 s) were made through the implanted cannulae and electrodes to mark the recording and infusion sites. The animals were

then perfused transcardially with ice-cold saline (0.9%) followed by 10% (vol/vol) formalin. The perfused brain was left in 10% (vol/vol) formalin overnight. Coronal sections (80 μm) were prepared using a vibrating microtome (VT 1200S, Leica Microsystems, Wetzlar, Germany) and mounted on gelatin-coated glass slides. Sections were stained with 0.2% (wt/vol) cresyl violet solution and mounted with DPX. The slides were imaged to identify and reconstruct recording and infusion sites. 2 rats were excluded from the study due to incorrect positioning of the electrode bundles (Figure 1). Another 11 rats were excluded due to incorrect placement of either or both the electrodes and infusion cannulae (Figure 6).

In vitro coronal slice preparation

Rats were anaesthetized using halothane, decapitated and their brains were quickly dissected out and transferred to oxygenated, ice-cold cutting solution containing (in mM): 75 sucrose, 86 NaCl, 25 glucose, 2.5 KCl, 1.2 NaH_2PO_4, 25 $NaHCO_3$, 3.3 HEPES, 7 $MgCl_2$, 0.5 $CaCl_2$; equilibrated with 95% O_2 and 5% CO_2, pH 7.3, 305-310 mOsm. Acute coronal brain slices (400 μm thick) containing the amygdala were obtained in the cutting solution using a vibrating microtome (VT 1200S, Leica Microsystems), transferred to a submerged holding chamber and allowed to recover for 1 h at room temperature.

Whole-cell recordings

Slices were transferred to a submerged recording chamber (maintained at 28 ± 2°C) and perfused at a flow rate of 1.5-2 ml/min with oxygenated artificial cerebrospinal fluid (ACSF) consisting of (in mM): 115 NaCl, 25 glucose, 25.5 $NaHCO_3$, 1.05 NaH_2PO_4, 3.3 KCl, 2 $CaCl_2$ and 1 $MgSO_4$. LA principal neurons were visually identified using an upright differential interference contrast microscope (BX50WI, Olympus, Tokyo, Japan). Patch pipettes (3-5 MΩ resistance), pulled from thick walled Borosilicate glass using a P1000 Flaming/Brown micropipette puller (Sutter Instruments, Novato, CA, USA) and filled with an internal solution containing (in mM) 120 K-gluconate, 20 KCl, 10 HEPES, 4 NaCl, 4 MgATP, 0.3 NaGTP, 0.2 EGTA and 10 phosphocreatine (pH 7.4, ~285 mOsm) were used to patch on to principal neurons in the LA. In experiments where evoked responses were recorded, a bipolar electrode (25 μm diameter Platinum/Iridium, FHC, Bowdoin, ME, USA) connected to an ISO-Flex stimulator (A.M.P.I., Jerusalem, Israel) was used to stimulate the internal capsule containing the thalamic inputs to the amygdala. For all recordings, neurons were held at −70 mV. Neurons were used for recording if the initial resting membrane potential (V_m) < −60 mV and series resistance (R_s) between 15-25 MΩ. Neurons that exhibited more than a 20% change in R_s during the recording were not included for analysis. Data were acquired using an EPC-9 amplifier (HEKA Elektronik GmbH, Lambrecht/Pfalz, Germany), filtered at 2.9 kHz (Bessel filter) and digitized at 20 kHz. Data acquisition and current injections were performed using the Patchmaster software (HEKA Elektronik GmbH). Electrophysiological data were analyzed using custom-written programs in IGOR Pro (WaveMetrics, Portland, OR, USA), unless otherwise stated.

Long-term potentiation (LTP)

Evoked responses of neurons in the lateral amygdala (LA) were recorded in response to stimulation of internal capsule fibers containing thalamic inputs to the LA (at 0.05 Hz). In the 'DHPG' groups (Figures 5A–5C), 100 μM DHPG was bath applied to the slices for 10 min after transferring to the recording chamber. Following this, a 5 min stable baseline was recorded, at 0.05 Hz and LTP induced at the thalamic inputs no later than 30 mins after termination of DHPG incubation. LTP was induced by application of 2 trains of 100 pulses, each at 30 Hz frequency. Post LTP induction, EPSPs were recorded for 30 min at 0.05 Hz. LTP was quantified in Igor Pro (WaveMetrics) by measuring the initial slope of the EPSP, calculated during a 1-2 ms period, by placing cursors within the 10 to 90 range of the baseline EPSP slope. The same cursor settings were maintained for slope measurements over the entire pre and post-LTP time course for each cell. The measured EPSP slopes were then normalized to the average baseline value for each cell. For statistical comparison, EPSP slope values normalized to baseline, during the 25-30 min period after LTP induction was compared across groups.

Miniature excitatory postsynaptic current (mEPSC) recordings

mEPSCs were recorded in voltage-clamp mode using an internal solution containing (in mM): 110 gluconic acid, 110 CsOH, 20 CsCl, 0.2 EGTA, 10 HEPES, 4 NaCl, 4 Mg-ATP, 0.3 Na-GTP, 10 phosphocreatine, 5 QX-314 (pH 7.4; ~295 mOsm). mEPSCs were isolated in the presence of picrotoxin (75 μM) and TTX (0.5 μM) in the perfusate. 10μM of 3-[(2-methyl-1,3-thiazol-4-yl) ethynyl] pyridine (MTEP) was added to the perfusate when required to inhibit mGluR5. In experiments where post-synaptic Ca^{2+} was chelated out (Figures 4E and 4F), BAPTA (1,2-bis(*o*-aminophenoxy)ethane-*N,N,N',N'*-tetraacetic acid, 10 mM) was added in the internal solution. Baseline current traces of 5 min duration (beginning at least 5 minutes after achieving whole-cell configuration) were recorded. 100 μM of DHPG was applied in the bath solution for 10 minutes and then washed out for 30 min. Baseline synaptic activity was determined by analyzing 5 min of continuous current traces immediately before DHPG application. To study the effect of DHPG on the mEPSCs, 5 min of recordings were analyzed during the drug application and the last 5 min of the DHPG washout recordings were analyzed to assess the post-DHPG synaptic release. Mini Analysis Program (Synaptosoft Inc., Decatur, GA, USA) was used for analyzing the traces. One outlier sample (> 2 SD) was excluded from the *Fmr1*$^{-/y}$ group in Figures 2C and S2.

Paired-pulse ratios

Evoked EPSCs from principal neurons in the LA were obtained upon stimulation of the internal capsule containing thalamic inputs to the LA. A pair of stimuli was delivered with an interstimulus interval of 25ms and the responses averaged across 10 trials. Paired-pulse

ratios (PPRs) were determined as the ratio of the amplitude of the second EPSC to the first. After recording baseline PPRs, 100 μM DHPG was washed onto slices for 10 min. PPRs were measured again during DHPG incubation as well as after a 15 min washout.

Biochemical analysis of surface and total GluA1

Coronal slices were obtained as described above and allowed to recover at RT for 1h in ACSF containing (in mM): 115 NaCl, 25 glucose, 25.5 $NaHCO_3$, 1.05 NaH_2PO_4, 3.3 KCl, 3.3 HEPES, 2 $CaCl_2$ and 1 $MgSO_4$. Slices were then transferred to a chamber with 50μM DHPG for 10 min at RT followed by incubation with 0.6mg/ml biotin (EZ-Link™ Sulpho- NHS-SS-Biotin, Thermo Fisher, Waltham, MA, USA) at 4°C for 45 min. Ice cold 25mM Tris-ACSF was added to stop the biotinylation reaction. The BLA was micro-dissected out, flash-frozen and stored at −80°C. The tissue were homogenized in RIPA buffer containing 50mM Tris-HCl, 1% TritonX, 0.5% Na-deoxycholate, 0.1% SDS, 150mM NaCl, 50mM NaH_2PO_4, 2mM EDTA, 2X protease inhibitor cocktail, 1X phosphatase inhibitor cocktail 2, and phosphatase inhibitor cocktail. 100 μg of each sample was incubated overnight with 40mg of precleared Neutravidin beads at 4°C. The beads were washed three times with RIPA buffer. Finally, 40ul of 2X laemmli buffer (20% glycerol, 4% SDS, 125mM ris-HCl, PH-6.8, 0.004% bromo-phenol Blue, 1% beta mercapto-ethanol) was added to the beads, heated at 90°C for 5 min and spun down. 10ul of the supernatant was loaded and separated in a precast gradient gel (NuPAGE 4%–12% Bis-Tris Protein Gels, Thermo Fisher). The resolved proteins were transferred to nitrocellulose membrane in a Bio-Rad transfer apparatus. Membranes were washed with 1X Tris-buffered saline (TBS) and blocked with 1:1 TBS: Odyssey Blocking Buffer (LI-COR Biosciences, Lincoln, NE, USA) containing 0.1% Tween20 for 1h at RT followed by incubation with primary antibodies (1:1000 anti-GluA1, Millipore, RRID:AB_11212678 ; 1:1000 anti-avidin, RRID:AB_557672, Thermo Fisher) overnight at 4°C. After washing with 1X TBST, the membranes were incubated for 1 h with secondary antibodies (1: 10,000 IRDye 800CW goat anti-rabbit IgG; 1: 10,000 IRDye 680LT goat anti-mouse IgG; LI-COR Biosciences) at RT followed by washes in 1X TBST. The immunoblots were dried and digitally scanned by using the Fc Odyssey Infrared Imaging System, (LI-COR Biosciences). Densitometric analysis was performed with the help of the Li-Cor Image Studio Lite software.

Immunofluorescence in tissue sections

Brain sections were incubated in 4% goat serum + 0.5% Triton X-100 for 4 h. Primary antibody staining (1:500 anti-RIM1, RRID:AB_2661872; 1:500 anti-Homer1, RRID:AB_10549720; Synaptic Systems; 1:500 anti mGluR5, RRID:AB_1619239; Neuromics) was carried out overnight in the same buffer at 4°C. Samples were washed 5x in PBS before carrying out secondary antibody staining for 3 h at room temperature.

Expansion microscopy

Following immunofluorescence labeling, samples were treated with Acryloyl-X-SE (Thermo Fisher) overnight at RT. 200 μl of monomer solution was added to the coverslip and gelation was carried out at 37°C for 1 h. Tissue sections were pre-incubated in monomer solution at 4°C for 30 min, prior to transferring the samples to 37°C for 2 h to allow gelation to occur. Following ProteinaseK digestion overnight, slightly expanded gels were transferred to a larger dish and water exchange was performed until gels were fully expanded. Expanded gels were transferred into 50x7 mm glass bottom dishes for imaging. Expanded gels were imaged using Zeiss (Jena, Germany) LSM780/880 confocal microscopes and a 40x oil objective (NA 1.3, PSF: LSM780- 0.217/0.260/0.566 μm; LSM880- 0.238/0.253/0.636 μm x/y/z). Z stacks (0.37 μm 63x/ 0.43 μm 40x) spanning the entire volume of tissue were obtained and analyzed using Imaris (Bitplane, Zürich) and ImageJ.

Image analysis

The maximum intensity projections of both the amygdala and hippocampus were assessed in order to evaluate the position of mGluR5 relative to pre (RIM1) and post-synaptic (Homer1) markers (Hafner et al., 2019). Line scan analysis was performed through single synapses where both synaptic signals (mGluR5 & either RIM1/Homer1) were present. Only signals where a 1μm x 1μm ROI fully encompassed adjacent/co-localized signals were included for analysis. Performing a line scan of a 1 μm ROI through the signals of interest, the intensity distribution for over 200 individual synapses were assessed per condition/per experiment. The peak-to-peak distance was then calculated for the sum of all the assessed pairs for each experiment.

QUANTIFICATION AND STATISTICAL ANALYSIS

For all plots, 'n' denotes the number of neurons while 'N' denotes number of rats, unless otherwise stated. All figures represent mean ± SEM (except the cumulative probability graphs). All statistical tests were performed using GraphPad Prism (GraphPad Software Inc., San Diego, CA, USA) and are included in the figure legends. Data points deviating more than 2 SD values from the mean were excluded from the analyses. All datasets passed a test for normality (D'Agostino-Pearson test) and significance was determined using parametric tests (with an exception of the KS test) with an alpha value of 0.05. All tests were performed using a two-tailed design, assumption of equal variances and corrected for multiple comparisons. Sample sizes were not determined prior to the experiments and were sufficient to get significant effects.